

Meeting the Cool Neighbors III: Spectroscopy of Northern NLTT Stars

K. L. Cruz¹

Department of Physics and Astronomy, University of Pennsylvania, 209 South 33rd Street, Philadelphia, PA 19104

kelle@sas.upenn.edu

and

I. Neill Reid¹

*Space Telescope Science Institute, 3700 San Martin Drive, Baltimore, MD 21218;
Department of Physics and Astronomy, University of Pennsylvania, 209 South 33rd Street, Philadelphia, PA 19104*

inr@stsci.edu

ABSTRACT

We present initial results of an all-sky search for late-type dwarfs within 20 pc of the Sun using the New Luyten Two-Tenths (NLTT) catalog cross-referenced with the 2-Micron All Sky Survey (2MASS) database. The results were obtained with low-resolution optical spectroscopic follow-up of candidate nearby-stars as a preliminary test of our methodology. M_J , derived using spectral indices, and 2MASS J are used to estimate distances. Out of the 70 objects observed, 28 are identified as previously unrecognized objects within 25 pc of the Sun, and up to 19 of these are within 20 pc. One, LP 647-13 is an M9-type dwarf at 10.5 pc making it one of the four closest M9 dwarfs currently known. We also discuss the chromospheric activity of the observed dwarfs.

Subject headings: galaxy: stellar content — Solar Neighborhood — stars: distances — stars: late-type dwarfs

¹Visiting Astronomer, Kitt Peak National Observatory, National Optical Astronomy Observatory, which is operated by the Association of Universities for Research in Astronomy, Inc. (AURA) under cooperative agreement with the National Science Foundation.

1. Introduction

This is the third in a series of papers which present the results of our survey of the low-mass residents of our immediate Solar Neighborhood. Reid & Cruz (2002, hereafter Paper I) discussed how our capabilities for finding low-luminosity main-sequence stars has been enhanced with the availability of the 2-Micron All Sky Survey (2MASS) (Skrutskie 2001). The method that we focus on in this paper is using 2MASS in conjunction with proper-motion catalogs — particularly the New Luyten Two-Tenths (NLTT) catalog (Luyten 1979). This strategy is one part of a comprehensive search for previously-unrecognized nearby stars. The goals of the project are two-fold: to identify late-type dwarfs within 20 pc that can be targeted for detailed study as part of the NSF/NStars project and to use this sample to determine the mass function of low-mass objects in the Galactic Disk.

Our first results have come from targeting high proper-motion objects from the NLTT catalog. As discussed in Paper I, we were able to identify a substantial fraction of the proper-motion stars in the 2MASS database based on location coincidence. With this sample, we are able to select candidate nearby dwarfs by combining the m_r estimates from the NLTT and the near-infrared magnitudes provided by 2MASS and using $m_r - K_s$ colors to obtain a rough photometric distance.

As detailed in Paper I, our initial sample of nearby-star candidates is drawn from NLTT objects that have a 2MASS counterpart within a $10''$ search radius. While 23,795 objects were found, only 1245 have photometric properties consistent with their being late-type dwarfs within 20 pc of the Sun. This sample is dubbed NLTT Sample 1.

NLTT Sample 1 has already yielded many previously unrecognized nearby objects. In Paper I, we combine the 2MASS infrared magnitudes with published optical photometry for 469 dwarfs, identifying 76 additions to the 20 pc sample. Reid, Kilkenny & Cruz (2002, hereafter Paper II) lists 48 new objects within 20 pc, five of which are probably within 10 pc. These were located by obtaining optical photometry of 180 bright southern nearby-star candidates with the facilities at the Sutherland station of the South African Astronomical Observatory.

This paper presents the first results from spectroscopic follow-up observations of NLTT stars. The selection of the current sample and its overlap with the finalized NLTT Sample 1 are outlined in §2. Section 3 describes our observations. We present spectral indices, spectral types, absolute magnitudes, and distances for all the observed objects in §4. A discussion of our findings, particularly interesting objects, and chromospheric activity is in §5. We summarize the main results in the final section.

2. Target Selection

The objects presented in this paper are taken from the initial sample of 23,795 NLTT objects that have a 2MASS counterpart within $10''$ of the NLTT position and $|b| > 10^\circ$, but were selected before we finalized the criteria for defining the NLTT Sample 1. Indeed, these observations provided some of the basis for those criteria.

The present set of targets were required to have declinations greater than -30° and right ascensions between 21^{h} and 5^{h} . The following color criteria further reduced the sample to 907 objects:

$$m_r(\text{lim}) = \begin{cases} 1.67(m_r - K_s) + 5.5, & \text{if } 1.5 < (m_r - K_s) \leq 3, \\ 5(m_r - K_s) - 4.5, & \text{if } 3 < (m_r - K_s) \leq 3.8, \\ 1.72(m_r - K_s) + 8, & \text{if } 3.8 < (m_r - K_s) \leq 7. \end{cases} \quad (1)$$

Objects were eliminated if $m_r > m_r(\text{lim})$.

Primary and secondary target lists were created by invoking stricter color criteria, designed to probe areas of color-space most likely to contain nearby, late-type objects. The primary list includes 52 objects which meet the above criteria and have $J - K_s$ colors redder than 0.95 and $H - K_s > 0.35$. The $J - K_s$ cut eliminated 628 objects while the $H - K_s$ eliminated 818. The secondary list includes 119 targets, all with $R - K_s > 5$. Taking into account the significant overlap between the two lists, there is a total of 127 target objects. Twenty-nine already have spectroscopic observations, with most identified as mid to late M-dwarfs (Table 1). Twenty-eight objects were eliminated because the 2MASS magnitudes were unreliable due to nearby bright stars or their diffraction spikes, unresolved companions, or an NLTT/2MASS mismatch. A mismatch occurs when more than one 2MASS object is within $10''$ of the NLTT position and the NLTT object is linked with both the correct and incorrect 2MASS objects (see Paper I, §3.3). In some cases, we were able to correct the mismatches and observe the appropriate object. The resulting target list includes 70 objects — all of which we observed and present here².

Following this initial observing run, we were able to refine our color criteria to more efficiently exclude objects beyond 20 pc. The finalized criteria are described in Paper I and were used to create the NLTT Sample 1 consisting of 1245 targets. These observations include a significant number of targets lying beyond the 20 parsec limit. In Figure 1, we

²Finder charts can be obtained from the 2MASS Survey Visualization and Image Server at <http://irsa.ipac.caltech.edu/> using the positions or names given in Tables 2 and 3.

show all of the observed objects with the finalized (m_r , $R - K_s$) color criteria superimposed (see Paper I, §3.2). Objects in the NLTT Sample 1 are listed in Table 2, while data for targets which fail to meet our final selection cut are presented in Table 3.

3. Observations

We obtained optical spectroscopy of our sample with the Kitt Peak National Observatory 2.1 m telescope using the GoldCam CCD Spectrograph. We employed a 400 line mm^{-1} grating blazed at 8000 Å with a 1''.3 slit to give a resolution of 5.1 Å (2.8 pixels) over the wavelength range 5500–9300 Å. We used an OG-550 blocking filter to block higher orders. The observations were taken over four nights from 2000 September 29 through October 2 (UT), all under photometric conditions and with good seeing (between 1'' and 1''.5).

The spectra were extracted and wavelength and flux calibrated using standard IRAF routines. We used zero-second dark exposures taken at the beginning of each night to remove the bias level from each exposure, via the IRAF routine CCDPROC, which was also used to fix bad pixels. All spectra were extracted using APALL. Wavelength calibration was determined from HeNeAr arcs taken after each exposure. The spectra were flux calibrated using observations of HD 19445 (Oke & Gunn 1983), and the spectral ratios were measured using IDL scripts.

The CCD used with GoldCam suffers from fringing in the red which has an amplitude of $\pm 3\%$ at 8000 Å, rising to $\pm 10\%$ at 8400 Å. In an attempt to compensate for this effect, an internal-lamp flat-field exposure was taken after each stellar observation. However, we were unable to use these data to correct the observed fringing in a satisfactory manner. Since the fringing does not affect the spectrum in the regions sampled by the measured bandstrength indices, and since there are no significant flat-field features shortward of 7800 Å, we have not applied flat-field corrections to the data.

4. Results

The change in strength of the major features present in spectra of late-type stars is tied to variation in effective temperature. Thus, we use measurements of the strengths of those features to estimate spectral type and absolute magnitude. Band strengths can be quantified by measuring spectral ratios or indices. Table 4 defines the spectral indices used in our study. These are taken from Reid, Hawley, & Gizis (1995a, hereafter PMSU1), Kirkpatrick et al. (1999), and Martín et al. (1999), and are designed to measure the strengths of the most

prominent features of M and early L-type dwarfs. The indices are calculated by taking the ratio between the summed flux in a region that contains an atomic or molecular feature and the summed flux in a nearby region that approximates the local pseudo-continuum. Table 5 lists the measurements for all of the observed objects.

4.1. Metallicity

In late-type dwarfs the relative strength of CaH and TiO absorption provides a metallicity indicator, with TiO absorption decreasing more rapidly than CaH with decreasing metal abundance (Mould 1976). Gizis (1997) used this behavior to define a classification system for late-type subdwarfs, classifying stars as either subdwarfs, sdM (intermediate abundance, $[\text{Fe}/\text{H}] \sim -1$), or extreme subdwarfs, esdM ($[\text{Fe}/\text{H}] < -1.5$). Figure 2 plots the CaH 1-TiO 5 and CaH 2-TiO 5 diagrams for our sample, where data for the reference stars are taken from PMSU1 (the disk main sequence) and Gizis (1997, sdM and esdM sequences). All of our targets, except LP 410-38 (2M0230) and LP 702-1 (2M2310), have spectral indices consistent with their being near solar-abundance disk dwarfs. These two objects are further discussed in §5.2. While the location of LP 824-383 (2M0012) in the CaH 2-TiO 5 plane is consistent with that of an intermediate subdwarf, the spectrum has a low signal-to-noise ratio and the CaH 1 and CaH 2 measurements are not reliable.

4.2. Spectral Types

We have defined the spectral type calibration using data for nearby stars and brown dwarfs with published spectral types (Kirkpatrick et al. (2000); PMSU1). We have supplemented our own observations with Keck Low-Resolution Infrared Spectrometer (Oke et al. 1995, LRIS) spectra of late-M and L dwarfs obtained by INR and collaborators as part of the 2MASS Rare Object Project³. Spectral ratios for the standards were measured using the same scripts used for the KPNO data presented here. The indices that best correlate with spectral type are TiO 5 and VO-a. Both indices are double-valued, with TiO 5 reversing in strength at M7 and VO-a at M9. For the early TiO 5 sequence, we adopt the relation found by PMSU1. The data and the calibration curves are plotted in Figure 3.

³Most of the spectra are publicly available from <http://dept.physics.upenn.edu/~inr/>

The spectral type calibration relations are:

$$S_p = -10.775(\text{TiO 5}) + 8.200, \quad (\text{TiO 5}) \leq 0.75, \quad \sigma = 0.5 \text{ subclasses},$$

$$S_p = 5.673(\text{TiO 5}) + 6.221, \quad (\text{TiO 5}) \geq 0.3, \quad \sigma = 0.38 \text{ subclasses, 23 stars},$$

$$S_p = 10.511(\text{VO-a}) - 16.272, \quad \sigma = 0.82 \text{ subclasses, 59 stars},$$

$$S_p = -7.037(\text{VO-a}) + 26.737, \quad \sigma = 0.50 \text{ subclasses, 22 stars.}$$

In principle, these relations yield up to four estimates of the spectral type. However, the fact that the two indices' trends reverse at different spectral types allows us to resolve the ambiguity since only one pair of solutions agree. We take the spectral type to be the weighted average of the results (one from TiO 5 and one from VO-a) rounded to the nearest half spectral type. The resulting uncertainty is ± 0.5 subclasses.

4.3. Absolute Magnitudes and Derived Distances

The absolute magnitude/band strength calibration was defined using a sample of 68 late-type dwarfs (from K5 to M7) with well-determined trigonometric parallaxes, taken from the nearby stars surveyed by PMSU1. The latter authors provide band strength measurements for a variety of indices. We find that color-magnitude diagrams using the TiO 5, CaH 2, and CaOH indices show the smallest dispersion in the main sequence, and hence the best prediction of absolute magnitude. The calibrating data and curves are shown in Figure 4.

There is a jump in all three color-magnitude diagrams at $M_J = 8.5$. This break is discussed in detail in §4.2 of Paper I. To accommodate this jump, we have fit the main sequence in two separate regions. The absolute magnitude calibration relations are:

$$M_J = 2.79(\text{TiO 5})^2 - 7.75(\text{TiO 5}) + 10.49, \quad (\text{TiO 5}) \geq 0.34, \quad \sigma = 0.35 \text{ mag., 46 stars},$$

$$M_J = -7.43(\text{TiO 5}) + 11.82, \quad (\text{TiO 5}) \leq 0.43, \quad \sigma = 0.19 \text{ mag., 22 stars},$$

$$M_J = 6.50(\text{CaH 2})^2 - 13.24(\text{CaH 2}) + 12.10, \quad (\text{CaH 2}) \geq 0.36, \quad \sigma = 0.33 \text{ mag., 46 stars},$$

$$M_J = -9.33(\text{CaH 2}) + 12.50, \quad (\text{CaH 2}) \leq 0.42, \quad \sigma = 0.19 \text{ mag., 20 stars},$$

$$M_J = 5.67(\text{CaOH})^2 - 11.99(\text{CaOH}) + 11.82, \quad (\text{CaOH}) \geq 0.36, \quad \sigma = 0.32 \text{ mag., 46 stars},$$

$$M_J = -7.31(\text{CaOH}) + 11.80, \quad (\text{CaOH}) \leq 0.43, \quad \sigma = 0.28 \text{ mag., 21 stars.}$$

As with the spectral type calibration, there is a region of overlap between the relations for each spectral index where M_J is ambiguous. These regions ($0.34 \leq \text{TiO 5} \leq 0.43$,

$0.36 \leq \text{CaH 2} \leq 0.42$, $0.36 \leq \text{CaOH} \leq 0.43$) are enclosed by dashed boxes in Figure 4. The calibration objects that lie in these regions are mostly M3.5-, M4-, and M4.5-type dwarfs. The measured spectral ratios give an unambiguous estimate of M_J for most of the NLTT dwarfs. However, in a few cases, one or all of the predictions for M_J are multi-valued (there are no cases where two of the three indices give ambiguous predictions). In cases where only one index yields two values for M_J , we adopt the value that is the closest to the predictions from the other two spectral ratios. The value is included in the weighted average of M_J if it lies within 3σ of either of the other two values. In the case of all three indices yielding two values for M_J , we quote all six values and compute two weighted averages using the sets of predictions that are closest to each other. We therefore give two estimates of M_J and thus, two estimates for the distance for a small number of stars in Tables 2 and 3 (e.g., G 75-35 (2M0241) in Table 2). Reliable distances for these objects can only be derived by obtaining trigonometric parallaxes.

The uncertainty in M_J was calculated by adding in quadrature two contributions to the uncertainty: the RMS of the weighted average based on the RMS of the individual calibration fits stated above and the standard deviation of the values of M_J given by the different spectral ratios. Using this scheme and the 2MASS apparent J magnitude, we estimate M_J and the distance to all of our (disk dwarf) targets (Tables 2 and 3).

5. Discussion

5.1. Additions to the Nearby-Star Sample

Our spectroscopic observations confirm that combining optical and near-infrared photometry is an effective means of identifying new stellar neighbors, even when the optical photometry is as unreliable as the magnitudes listed in the NLTT catalog. In particular, of the 35 stars listed in Table 2, selected on the basis of our finalized color-magnitude criteria, up to 19 (54%) are likely to lie within 20 pc of the Sun, while up to 27 (77%) probably lie within the 25 pc sample. Several stars require particular comment.

5.1.1. LP 647-13

At spectral type M9, LP 647-13 (2M0109) is the latest of the NLTT dwarfs in the present sample, falling beyond the range of validity of the absolute magnitude calibrations plotted in Figure 4. Figure 5 compares our spectrum of this object with Keck LRIS data for the M9 standard LHS 2065 and the M9.5 standard BRI 0021-0214. There are obvious

strong similarities between LP 647-13 and LHS 2065. Kirkpatrick, Henry, & Simons (1995) list absolute magnitudes for these two standard stars and for two other M9 dwarfs in the immediate Solar Neighborhood: $M_K = 10.33$ for LHS 2065; $M_K = 10.22$ for BRI 0021; $M_K = 10.46$ for LHS 2924; and $M_K = 10.24$ for TVLM 868-110638. A straight average gives $M_K = 10.31 \pm 0.11$ magnitudes. Applying that value gives a distance of only 10.5 pc to LP 647-13, making it one of the four closest M9 dwarfs currently known, along with LHS 2065 at 8.5 pc, LHS 2924 at 10.5 pc, and DENIS-P J104814.7–395606.1 at ~ 5 pc (Delfosse et al. 2001).

5.1.2. LP 763-38

This dwarf (2M2337) has spectral indices which place it at the extreme limit of validity of our calibration. Figure 6 plots our spectral data and compares those with the M7 standard, VB 8 (Gl 644C). Given the strong similarities, we classify LP 763-38 as spectral type M7, and estimate the distance using VB 8 ($M_K=9.76$) as a template. Matching that value against the observed K magnitude of 11.206 for LP 763-38 gives a distance modulus of 1.47 magnitudes, or a distance estimate of 20.0 ± 3.0 pc.

5.2. Possible Subdwarfs: LP 410-38 & LP 702-1

As discussed above, our band-strength measurements suggest that these two stars (2M0230 and 2M2310, in Table 3) are intermediate-abundance subdwarfs. Figure 7 compares our spectra against data for LP 890-2 (2M0413, Table 2), an M6 dwarf in our NLTT sample, and LHS 377, one of the coolest-known intermediate subdwarf (sdM7, Gizis (1997)). LP 702-1 is clearly similar to LP 890-2, suggesting that the subdwarf-like spectral indices may reflect the relatively low signal-to-noise ratio of our spectrum. LP 410-38, on the other hand, has spectral characteristics which are closer to LHS 377, notably the enhanced CaH absorption at 6400 and 7000 Å. We therefore classify LP 702-1 as an M6, near-solar abundance disk dwarf, but identify LP 410-38 as an intermediate subdwarf, spectral type sdM6. We adopt $M_J = 10.15 \pm 0.16$ for LP 702-1. This was computed by averaging the values of M_J for all of the M6-type dwarfs in our sample. This yields a distance estimate of 37.0 ± 5.0 pc. The Gizis (1997) subdwarf sample does not include any sdM6 stars, but both LHS 377 and LHS 407 (sdM5) have measured parallaxes (Monet et al. (1992) and Ruiz & Anguita (1993), respectively). Ruiz & Anguita (1993) also present JHK photometry for LHS 407, while Leggett et al. (2000) list such data for LHS 377. Combining those measurements gives $M_K = 9.74 \pm 0.4$ for LHS 377 and $M_K = 9.55 \pm 0.8$ for LHS 407. We therefore adopt $M_K = 9.7$ for LP 410-

38, giving a distance estimate of 18.0 ± 5.0 pc. We note that the H α emission evident in LP 410-38 is unusual, but not unprecedented, in late-type subdwarfs, and might reflect the presence of a close companion, as with Gl 455 and Gl 781 (Gizis 1997).

5.3. Chromospheric Activity

Chromospheric activity, as evidenced by emission at either the Ca II H & K lines or the Balmer series, is common among late-type dwarfs. A significant number of the NLTT dwarfs exhibit H α emission, as evidenced by H α indices exceeding 1.0 in Table 5. We have used the options available in the IRAF routine SPLOT to measure equivalent widths and line fluxes for 43 stars, and the results are listed in Table 6. Our observations set a typical upper limit of 0.75 Å on H α emission in the remaining stars. This fraction of $\sim 60\%$ is broadly consistent with the expected proportion of dMe dwarfs at spectral types of M5 to M6 (see Figure 6 in Gizis et al. (2000)).

Equivalent width is still often used to characterize the level of activity but, as pointed out originally by Reid, Hawley, & Mateo (1995b) and later by Basri & Marcy (1995), this approach fails to take into account the decreased continuum level in later-type stars. A more effective means of gauging the relative activity of dwarfs spanning a wide range of spectral types (temperatures) is to consider the fraction of the total flux emitted as line emission, specifically F_α/F_{bol} , where F_α is the total flux in the H α line.

Our spectra give a direct measure of F_α . In order to determine F_{bol} , we need to estimate bolometric corrections for the NLTT dwarfs. We can calculate the latter using data from Leggett et al. (2000) observations of 28 nearby M dwarfs with spectral types between M1 and M6.5. Figure 8 plots the J -band bolometric corrections for those stars as a function of both spectral type and TiO 5 index, taking the latter from PMSU1. Both correlations are well described by linear relations

$$BC_J = (1.658 \pm 0.021) + (0.050 \pm 0.005) \times \text{sp. type}, \quad \sigma = 0.036,$$

and

$$BC_J = (2.065 \pm 0.020) - (0.533 \pm 0.050) \times \text{TiO 5}, \quad \sigma = 0.037.$$

We have used the latter relation to estimate bolometric corrections for the NLTT dwarfs with spectral types M1 to M6.5; we adopt $BC_J=1.9$ magnitudes for later spectral types (Reid et al. 2001). Table 6 lists the resulting values of $\log F_\alpha/F_{bol}$ for dwarfs with measurable H α emission.

Figure 9 compares the distribution of activity amongst the present sample against data for nearby emission-line M dwarfs from Hawley, Gizis, & Reid (1996, hereafter PMSU2).

2M0203 (LP 352-79) stands out as the most active star in the sample, with $\log F_\alpha/F_{bol} = -3.21$. We also note that Gizis et al. (2000) failed to detect H α emission in the M9 dwarf, 2M0350+1818, while we measure an H α equivalent width of 13.3 Å. Previous observations have shown that moderate-strength flares tend to occur with a duty cycle of a few percent amongst ultracool (spectral types later than M6.5) dwarfs (Reid et al. 1999; Martín & Ardila 2001), and this mechanism probably accounts for the relatively high levels of activity in both these dwarfs.

Considering the overall distribution in Figure 9, the (mainly) M5/M6 dwarfs observed in this paper are clearly less active, on average, than the dMe dwarfs in the PMSU sample. This is not unexpected, since recent studies indicate that the average level of activity is significantly lower amongst chromospherically-active ultracool dwarfs (Gizis et al. 2000; Basri 2001). Indeed, our observations bridge the gap between the ultracool datasets and the PMSU stars, which include few dwarfs between spectral types M5 and M7. Our data show that the average level of activity amongst dMe dwarfs falls from $\langle \log F_\alpha/F_{bol} \rangle = -3.9$ at spectral types earlier than M5 to $\langle \log F_\alpha/F_{bol} \rangle \sim -4.25$ for M5.5 dwarfs. Activity declines even further at later types, with $\langle \log F_\alpha/F_{bol} \rangle \sim -5$ at spectral type M9 and only 10 to 20% of early-type L dwarfs having detectable H α emission.

6. Summary

We have presented spectroscopic observations of 70 late-type dwarfs selected from the NLTT proper motion catalog as probable members of the immediate Solar Neighborhood based on their optical/near-infrared photometric properties. Of these 70 objects, 28 are found to be previously unrecognized stars within 25 pc of the Sun; 13 lie within 20 pc.

In addition to identifying a small sample of new members of the local stellar community, the observations described in this paper lay the foundations for the analysis of future observations. We have identified and calibrated a number of narrowband spectral indices which can be used to determine spectrophotometric parallaxes and spectral types for M dwarfs. Based on those calibrations, we have refined the photometric selection criteria used to identify candidate nearby stars from our cross-referencing of the NLTT catalog against the 2MASS database. Future papers will apply the techniques outlined in this paper to spectroscopic observations of a larger sample of nearby-star candidates.

This research was supported partially by a grant from the NASA/NSF NStars initiative, administered by JPL, Pasadena, CA. KLC acknowledges support from a NSF Graduate Research Fellowship. This research has made use of the SIMBAD database, operated at CDS, Strasbourg, France and the NASA/IPAC Infrared Science Archive, which is operated

by the JPL, California Institute of Technology, under contract with NASA. We would also like to thank our telescope operators at KPNO, Bill Gillespie and Hillary Mathis. This publication makes use of data products from the Two Micron All Sky Survey, which is a joint project of the University of Massachusetts and the Infrared Processing and Analysis Center/California Institute of Technology, funded by NASA and the NSF.

REFERENCES

Basri, G. 2001, in *ASP Conf. Ser.* 223, 11th Cambridge Workshop on Cool Stars, Stellar Systems and the Sun, ed. R. J. Garcia Lopez, R. Rebolo, & M. R. Zapatero Osorio (San Francisco: ASP), 261

Basri, G. & Marcy, G. W. 1995, *AJ*, 109, 762

Delfosse, X. et al. 2001, *A&A*, 366, L13

Dahn, C. et al. 2000, in *ASP Conf. Ser.* 212, From Giant Planets to Cool Stars, ed. C. A. Griffith & M. S. Marley (San Francisco: ASP), 74

ESA 1997, The Hipparcos Catalog, VizieR On-line Data Catalog: I/239

Gizis, J. E. 1997, *AJ*, 113, 806

Gizis, J. E., Monet, D. G., Reid, I. N., Kirkpatrick, J. D., Liebert, J., & Williams, R. J. 2000, *AJ*, 120, 1085

Gizis, J. E. & Reid, I. N. 1997, *PASP*, 109, 849

Gliese, W. & Jahreiß, H. 1991, Preliminary Version of the Third Catalog of Nearby Stars (pCNS3), (Greenbelt: NASA/Astronomical Data Center), VizieR On-line Data Catalog: V/70A

Harrington, R. S. & Dahn, C. C. 1980, *AJ*, 85, 454

Harrington, R. S. et al. 1985, *AJ*, 90, 123

Hawley, S. L., Gizis, J. E., & Reid, I. N. 1996, *AJ*, 112, 2799, VizieR On-line Data Catalog: III/198 (PMSU2)

Kirkpatrick, J. D., Henry, T. J., & Simons, D. A. 1995, *AJ*, 109, 797

Kirkpatrick, J. D. et al. 2000, *AJ*, 120, 447

Kirkpatrick, J. D. et al. 1999, *ApJ*, 519, 802

Leggett, S. K. 1992, *ApJS*, 82, 351

Leggett, S. K., Allard, F., Dahn, C., Hauschildt, P. H., Kerr, T. H., & Rayner, J. 2000, *ApJ*, 535, 965

Luyten, W. J. 1979, New Luyten Catalog of stars with proper motions larger than two tenths of an arcsecond (Minneapolis: University of Minnesota), VizieR On-line Data Catalog: I/98A (NLTT)

Martín, E. L. & Ardila, D. R. 2001, *AJ*, 121, 2758

Martín, E. L., Delfosse, X., Basri, G., Goldman, B., Forveille, T., & Zapatero Osorio, M. R. 1999, *AJ*, 118, 2466

Monet, D. G., Dahn, C. C., Vrba, F. J., Harris, H. C., Pier, J. R., Luginbuhl, C. B., & Ables, H. D. 1992, *AJ*, 103, 638

Mould, J. R. 1976, *ApJ*, 207, 535

Oke, J. B. et al. 1995, *PASP*, 107, 375

Oke, J. B., & Gunn, J. E. 1983, *ApJ*, 266, 713

Phan-Bao, N. et al. 2001, *A&A*, 380, 590

Reid, I. N. 1993, *MNRAS*, 265, 785

Reid, I. N. & Cruz, K. L. 2002, *AJ*, 123, 2806 (Paper I)

Reid, I. N., Gizis, J. E., Kirkpatrick, J. D., & Koerner, D. W. 2001, *AJ*, 121, 489

Reid, I. N., Hawley, S. L., & Gizis, J. E. 1995a, *AJ*, 110, 1838, VizieR On-line Data Catalog: III/198 (PMSU1)

Reid, N., Hawley, S. L., & Mateo, M. 1995b, *MNRAS*, 272, 828

Reid, I. N., Kilkenny, D. & Cruz, K. L. 2002, *AJ*, 123, 2822 (Paper II)

Reid, I. N., Kirkpatrick, J. D., Gizis, J. E., & Liebert, J. 1999, *ApJ*, 527, L105

Ruiz, M. T. & Anguita, C. 1993, *AJ*, 105, 614

Skrutskie, M. F. 2001, *BAAS*, 198, No.33.01

Tinney, C. G., Mould, J. R., & Reid, I. N. 1993, AJ, 105, 1045

Weis, E. W. 1991, AJ, 101, 1882

Table 1. Previously Known Objects in Our Sample of NLTT Targets.

LP/NLTT Name	Other Name	α (J2000)	δ	M_V	Ref _V	M_J	m_r	J	H	K_s	d (pc)	Ref _{π}	Ref _{ph}	Sp. Type	Ref _{sp}
292- 67	LHS 112	00 20 29.22	33 05 08.28	15.57	2	9.81 ± 0.10	15.2	10.312	9.734	9.347	12.6 ± 0.6	1		M5.5	2
349- 25		00 27 55.91	22 19 32.89	...		10.99 ± 0.36	17.0	10.608	9.970	9.561	8.5 ± 1.4		3	M8.0	3
766- 87 ^a	LHS 1146	00 46 20.44	-19 24 43.95	...		10.30 ± 0.17	18.2	12.694	12.094	11.711	30.2 ± 2.3		4	M6.0	4
BD+22 176B ^b	GL 53.1B	01 07 38.52	22 57 21.91	12.01	12	7.90 ± 0.05	...	9.494	8.899	8.693	20.8 ± 0.5	5		M3.0	6
768- 26	GL 65B	01 39 01.21	-17 57 02.62	15.60	6	9.21 ± 0.03	12.2	6.302	5.685	5.358	2.62 ± 0.04	7		M5.5	6
768- 27	GL 65A	01 39 01.21	-17 57 02.62	15.47	6	9.21 ± 0.03	12.7	6.302	5.685	5.358	2.62 ± 0.04	7		M5.5	6
468-199 ^a	LHS 1294	01 45 45.29	13 06 00.39	...		6.65 ± 0.16	18.0	12.783	12.088	11.755	168.9 ± 12.2		4	M1.5	4
30- 55	G 245-040	02 01 54.02	73 32 32.13	13.87	2	9.11 ± 0.68	14.1	9.252	8.669	8.382	11.2 ± 3.4		2	M4.5	2
469-118 ^c		02 08 12.22	15 08 43.23	13.37	4	...	14.4			M4.5	4
245- 10	LHS 1378	02 17 09.93	35 26 33.03	15.88	2	9.88 ± 0.02	14.7	9.965	9.355	9.974	10.4 ± 0.1	8		M5.0	2
245- 18	G 074-015	02 20 25.24	37 47 30.68	10.92	2	7.30 ± 0.68	17.0	8.954	8.312	8.098	22.5 ± 6.8		2	M2.5	2
411- 6	LHS 1443	02 46 34.85	16 25 11.44	15.98	6	10.09 ± 0.22	16.1	10.971	10.518	10.159	15.1 ± 1.5	6		M6.0	6
412- 31		03 20 59.65	18 54 23.26	...		11.39 ± 0.35	17.6	11.744	11.043	10.572	11.9 ± 1.9	9		M9.0	3
356-770		03 30 05.07	24 05 28.25	...		10.83 ± 0.36	18.1	12.357	11.745	11.361	20.5 ± 3.4		3	M7.0	3
413- 53		03 50 57.37	18 18 06.54	...		11.45 ± 0.36	19.2	12.951	12.222	11.763	20.2 ± 3.3		3	M9.0	3
593- 68	LHS 1604	03 51 00.03	00 52 44.11	17.19	6	10.43 ± 0.06	16.5	11.262	10.592	10.191	14.7 ± 0.4	8		M6.0	2
	GJ 1072	04 50 50.83	22 07 22.49	14.48	6	9.12 ± 0.05	14.7	9.863	9.339	8.998	14.1 ± 0.3	7		M5.0	2
759- 17		22 02 11.26	-11 09 45.98	17.8	12.364	11.714	11.357	...			M6.5	3
759- 25	BRI 2202-1119	22 05 35.76	-11 04 28.71	...		9.81 ± 0.31	16.7	11.682	11.060	10.726	23.9 ± 3.4	10		...	
699- 43 ^d	LHS 3762	22 08 39.06	-08 14 33.37	...		9.98 ± 0.20	17.9	12.645	12.099	11.730	34.2 ± 3.2		4, 11	M5.0	4
759- 82	Gl 852A	22 17 18.99	-08 48 12.08	13.31	2	8.93 ± 0.13	14.0	9.010	8.463	8.173	10.4 ± 0.6	7		M4.0	2
760- 3	LHS 523	22 28 54.40	-13 25 17.86	16.96	6	10.60 ± 0.12	16.1	10.780	10.231	9.846	10.9 ± 0.6	8		M6.5	6
460- 44		22 35 49.07	18 40 29.93	...		11.25 ± 0.36	17.9	12.458	11.826	11.333	17.7 ± 2.9		3	M7.0	3
345- 18		22 55 58.45	28 22 46.65	17.3	12.554	11.935	11.538	...			M6.0	3
402- 58		23 36 43.93	21 53 38.67	...		11.01 ± 0.36	18.1	12.761	12.101	11.708	22.7 ± 3.7		3	M7.0	3
R 248	Gl 905	23 41 55.00	44 10 40.80	14.78	2	9.40 ± 0.01	12.7	6.90	6.252	5.934	3.17 ± 0.02	7		M5.0	2
523- 55		23 49 48.99	12 24 38.76	...		11.01 ± 0.36	18.4	12.615	11.952	11.562	21.2 ± 3.5		3	M8.0	3
348- 11		23 58 29.03	27 02 05.71	17.7	12.759	12.078	11.699	...			M6.0	3

^aUsed TiO 5 and CaH 2 indices and our calibrations to find M_J and distance.

^bDistance based on trigonometric parallax for companion, GL 53.1A

^cThe system made up of two NLTT objects, LP 469-118 and its close companion G 035-027, are unresolved by 2MASS and the photometry is not reliable.

^dUsed TiO 5 and CaH 2 indices and our calibrations to find M_J and a distance estimate. Final estimate is average of this value with estimates based on optical photometry

Note. — Column 1 lists the designation from the NLTT catalog. Identifiers without prefixes are Luyten-Palmar (LP) Survey numbers. Other identifiers are R=Ross and BD=Bonner Durchmusterung. Column 2 lists alternate designations. Columns 3 and 4 list the position of the 2MASS source. Column 5 lists M_V and Column 6 gives the source. Column 7 gives the value of M_J obtained using our distance estimates. Column 8 lists the m_r given in the NLTT. Columns 9-11 list the infrared photometry from 2MASS. Column 12 lists the distance estimates, and Column 13 and 14 give the source of the trigonometric parallax or photometry upon which the distance estimate is based. Column 15 lists the spectral type and Column 16 gives the source.

References. — (1) Harrington et al. (1985); (2) PMSU1; (3) Gizis et al. (2000); (4) Gizis & Reid (1997); (5) ESA (1997); (6) Gliese & Jahreiß (1991); (7) Harrington & Dahn (1980); (8) Monet et al. (1992); (9) Dahn et al. (2000); (10) Tinney, Mould, & Reid (1993); (11) Reid (1993); (12) Weis (1991).

Table 2. Data for Targets Included in NLTT Sample 1.

NLTT/LP Name	Other Name	α (J2000)	δ	m_r	J	H	K_s	$M_J(\text{TiO 5})$	$M_J(\text{CaH 2})$	$M_J(\text{CaOH})$	M_J	d_{ph} (pc)	Sp. Type	20 pc?
405- 5	LHS 1060	00 21 16.44	18 43 56.02	15.7	11.352	10.758	10.400	9.86 ± 0.19	9.47 ± 0.19	9.68 ± 0.28	9.67 ± 0.20	21.8 ± 2.0	M5.0	?
645- 53		00 35 44.13	-05 41 10.20	14.9	10.717	10.084	9.716	9.65 ± 0.19	9.07 ± 0.19 ^a	9.39 ± 0.28	9.37 ± 0.27	18.8 ± 2.3	M5.0	Y
647- 13		01 09 51.17	-03 43 26.41	17.9	11.695	10.921	10.418	10.5 ± 3.0 ^e	M9.0	Y
467- 17		01 12 00.03	15 02 17.20	16.9	11.928	11.321	10.965	9.89 ± 0.19	9.27 ± 0.19	9.37 ± 0.28	9.54 ± 0.30	30.3 ± 4.1	M5.5	N
768-113	G 272-43	01 33 58.01	-17 38 23.63	13.7	8.876	8.268	8.003	7.63 ± 0.35	7.55 ± 0.33	7.80 ± 0.32 ^a	7.67 ± 0.22	17.5 ± 1.8	M3.5	Y
352- 79		02 03 28.65	21 34 16.95	16.7	11.634	11.027	10.700	9.72 ± 0.19	9.57 ± 0.19	9.01 ± 0.28 ^a	9.52 ± 0.33	26.7 ± 4.0	M5.0	N
649- 72	LHS 1363	02 14 12.51	-03 57 43.35	15.5	10.472	9.839	9.466	9.96 ± 0.19	9.57 ± 0.19	9.52 ± 0.28	9.72 ± 0.23	14.2 ± 1.5	M5.5	Y
649- 93		02 18 57.89	-06 17 49.73	19.2	12.920	12.186	11.860	10.19 ± 0.19	9.71 ± 0.19	7.66 ± 0.32 ^c	9.95 ± 0.28	39.6 ± 5.0	M6.0	N
	G 75-35	02 41 15.11	-04 32 17.75	14.2	9.181	8.566	8.269	8.99 ± 0.19	8.82 ± 0.19	9.08 ± 0.28	8.94 ± 0.16	11.2 ± 0.8	M4.0	Y
								7.94 ± 0.35	7.89 ± 0.33	8.14 ± 0.32	8.00 ± 0.22	17.3 ± 1.8		
651- 17	LHS 1450	02 50 02.39	-08 08 41.88	16.5	11.878	11.226	10.850	9.96 ± 0.19	9.54 ± 0.19	9.66 ± 0.28	9.73 ± 0.22	27.0 ± 2.7	M5.5	N
299- 15		03 05 07.86	27 42 27.94	16.3	11.602	11.023	10.636	9.55 ± 0.19	9.41 ± 0.19	9.15 ± 0.28 ^a	9.42 ± 0.20	27.4 ± 2.6	M5.0	N
888- 18		03 31 30.26	-30 42 38.19	18.2	11.371	10.699	10.276	10.21 ± 0.19	9.86 ± 0.19	6.82 ± 0.32 ^c	10.03 ± 0.22	18.6 ± 1.9	M6.0	Y
247- 56		03 38 18.63	38 28 56.03	17.0	11.962	11.338	11.003	9.79 ± 0.19	9.44 ± 0.19	9.43 ± 0.28	9.58 ± 0.21	30.0 ± 2.9	M5.0	N
31-301 ^d	G 221-27	04 05 57.40	71 16 41.00	13.9	9.542	8.983	8.716	8.88 ± 0.19	8.55 ± 0.19	8.71 ± 0.28	8.72 ± 0.18	14.7 ± 1.2	M4.0	Y
								7.86 ± 0.35	7.66 ± 0.33	7.76 ± 0.32	7.76 ± 0.21	22.9 ± 2.2		
31-302 ^d		04 05 56.50	71 16 38.55	15.1	10.125	9.547	9.234	9.66 ± 0.19	9.58 ± 0.19	9.67 ± 0.28	9.63 ± 0.13	12.6 ± 0.7	M5.0	Y
714- 37		04 10 48.10	-12 51 42.17	15.1	11.060	10.469	10.015	9.90 ± 0.19	9.45 ± 0.19	9.46 ± 0.28	9.63 ± 0.24	19.4 ± 2.1	M5.5	Y
890- 2 ^f		04 13 39.81	-27 04 29.14	18.4	12.214	11.578	11.190	10.13 ± 0.19	9.92 ± 0.19	9.63 ± 0.28	9.95 ± 0.24	28.5 ± 3.1	M6.0	N
775- 31		04 35 16.14	-16 06 57.52	17.4	10.396	9.780	9.336	10.26 ± 0.19	10.18 ± 0.19	9.78 ± 0.28	10.14 ± 0.24	11.3 ± 1.3	M6.0	Y
415-302	LHS 1690	04 39 31.60	16 15 44.85	15.0	10.120	9.539	9.187	9.86 ± 0.19	9.51 ± 0.19	9.67 ± 0.28	9.68 ± 0.19	12.3 ± 1.1	M5.0	Y
655- 48	1RXS	04 40 23.27	-05 30 08.29	16.4	10.681	9.985	9.557	10.00 ± 0.19	9.85 ± 0.19	9.19 ± 0.28	9.79 ± 0.37	15.3 ± 2.6	M6.0	Y
716- 10		04 52 04.01	-10 58 21.87	15.5	10.488	9.956	9.612	9.95 ± 0.19	9.40 ± 0.19	9.93 ± 0.28	9.72 ± 0.28	14.3 ± 1.8	M5.5	Y
396- 18		21 02 47.01	22 37 12.05	16.1	11.119	10.582	10.342	9.08 ± 0.19	8.53 ± 0.19	8.76 ± 0.28	8.79 ± 0.26	29.4 ± 3.5	M4.5	N
								8.01 ± 0.35	7.64 ± 0.33	7.81 ± 0.32	7.81 ± 0.24	46.2 ± 5.1		
397- 10		21 16 06.29	22 38 46.28	17.3	11.787	11.290	10.815	10.10 ± 0.19	9.81 ± 0.19	9.57 ± 0.28	9.88 ± 0.25	24.2 ± 2.8	M5.5	N
817- 54		21 29 23.39	-18 55 07.48	15.9	11.271	10.656	10.288	9.64 ± 0.19	9.39 ± 0.19	9.52 ± 0.28	9.51 ± 0.16	22.5 ± 1.6	M5.0	N
698- 2		21 32 29.74	-05 11 58.62	16.6	11.439	10.715	10.385	9.86 ± 0.19	9.42 ± 0.19	9.33 ± 0.28	9.58 ± 0.26	23.7 ± 2.8	M5.5	N
638- 50		21 51 27.01	-01 27 14.32	16.2	11.309	10.746	10.380	9.82 ± 0.19	9.64 ± 0.19	9.61 ± 0.28	9.71 ± 0.15	21.0 ± 1.5	M5.0	?
288- 40		22 36 01.58	36 55 51.34	18.2	12.155	11.552	11.286	9.44 ± 0.19	9.10 ± 0.19 ^a	9.43 ± 0.28	9.30 ± 0.20	37.4 ± 3.4	M4.5	N
521- 18	LHS 3856	22 48 22.45	12 32 10.54	15.9	11.206	10.627	10.226	9.81 ± 0.19	9.54 ± 0.19	9.42 ± 0.28	9.63 ± 0.20	20.8 ± 1.9	M5.5	?
401- 10		22 54 11.11	25 27 56.48	16.5	11.629	11.030	10.695	9.90 ± 0.19	9.81 ± 0.19	9.23 ± 0.28	9.74 ± 0.32	24.2 ± 3.5	M5.5	N
701- 59		23 01 50.86	-05 39 55.50	17.5	11.312	10.691	10.415	7.71 ± 0.35 ^a	7.38 ± 0.33	7.23 ± 0.32	7.43 ± 0.28	60.3 ± 7.7	M4.0	N
934- 33		23 22 23.63	-27 25 44.46	16.4	11.594	11.053	10.752	9.90 ± 0.19	9.71 ± 0.19	9.07 ± 0.28 ^b	9.80 ± 0.16	22.9 ± 1.7	M5.5	N
878- 90	G 275-42	23 23 36.58	-22 32 15.87	15.3	11.039	10.441	9.960	7.22 ± 0.35	7.14 ± 0.33	7.38 ± 0.32	7.25 ± 0.22	57.4 ± 5.7	M3.0	N
763- 38		23 37 14.93	-08 38 08.16	18.0	12.246	11.603	11.206	20.0 ± 3.0 ^e	M7.0	?

Table 2—Continued

NLTT/LP Name	Other Name	α (J2000)	δ	m_r	J	H	K_s	$M_J(\text{TiO 5})$	$M_J(\text{CaH 2})$	$M_J(\text{CaOH})$	M_J	d_{ph} (pc)	Sp. Type	20 pc?
763- 3		23 37 38.31	-12 50 27.60	16.7	11.461	10.851	10.427	10.00 ± 0.19	9.74 ± 0.19	9.52 ± 0.28	9.81 ± 0.23	21.5 ± 2.3	M5.5	?
239- 52		23 47 20.64	42 38 08.19	16.2	10.942	10.353	10.094	9.62 ± 0.19	9.15 ± 0.19^a	9.38 ± 0.28	9.38 ± 0.23	20.6 ± 2.2	M5.0	?

^aThis predicted value of M_J is double-valued and the result closest to the predictions based on other indices was used as our estimate M_J .

^bThis predicted value of M_J is double-valued and both predictions are more than 3σ from either of the other predictions. Neither are incorporated in calculating the final value M_J .

^cThis value is more than 3σ from either of the other predictions and was not used to estimate M_J .

^dLP 31-301 and LP 31-302 form a wide binary system with a separation of $5''$. The bandstrength indices measured for the brighter star fall in the ambiguous range, and we quote two distance estimates. The distance derived for the fainter star, LP 31-302, is consistent with the shorter distance of 14.7 ± 1.2 pc.

^eSee text for explanation of distance estimate.

^fAlso identified by Phan-Bao et al. (2001).

Note. — Column 1 lists the designation from the NLTT catalog. Identifiers without prefixes are Luyten-Palomar (LP) Survey numbers. Column 2 lists alternate designations. Columns 3 and 4 list the position of the 2MASS source. Column 5 lists the m_r given in the NLTT. Columns 6-8 list the infrared photometry from 2MASS. Columns 9-11 give the predicted M_J based on the spectral indices TiO 5, CaH 2, and CaOH. Column 12 gives our final estimate of M_J . Column 13 gives the distance estimates. Column 14 gives the spectral type. Column 15 indicates whether the object lies within our distance limit of 20 pc (Y), within 1σ of the boundary (?), or beyond the limit (N).

Table 3. Data for Targets Not Included in NLTT Sample 1.

NLTT/LP Name	Other Name	α (J2000)	δ	m_r	J	H	K_s	$M_J(\text{TiO 5})$	$M_J(\text{CaH 2})$	$M_J(\text{CaOH})$	M_J	d_{ph} (pc)	Sp. Type
704- 48		00 06 47.47	-08 52 35.22	17.0	11.970	11.409	11.059	10.27 ± 0.19	10.15 ± 0.19	10.27 ± 0.28	10.22 ± 0.13	22.4 ± 1.4	M6.0
880-442 ^d	G 267-33	00 07 22.50	-29 35 17.00	14.8	11.285	10.745	10.518	8.70 ± 0.19	8.50 ± 0.19	8.80 ± 0.28	8.64 ± 0.17	33.9 ± 2.7	M3.5
								7.72 ± 0.35	7.62 ± 0.33	7.85 ± 0.32	7.73 ± 0.21	51.6 ± 5.0	
880-441 ^d		00 07 22.50	-29 35 25.67	18.0	13.017	12.481	12.135	10.11 ± 0.19	9.64 ± 0.19	10.86 ± 0.28	10.06 ± 0.52	40.1 ± 9.4	M5.5
824-383 ⁱ		00 12 27.48	-25 28 00.72	18.9	13.155	12.543	12.092	9.81 ± 0.19	10.13 ± 0.19	5.65 ± 0.32^c	9.97 ± 0.21	43.6 ± 4.2	M5.5
150- 53		00 53 42.45	49 42 51.39	18.8	13.014	12.467	12.039	10.21 ± 0.19	9.98 ± 0.19	9.45 ± 0.28	9.97 ± 0.34	41.0 ± 6.4	M6.0
150- 58		01 00 44.37	50 55 44.76	17.9	12.476	11.881	11.504	10.00 ± 0.19	9.66 ± 0.19	9.64 ± 0.28	9.80 ± 0.21	34.5 ± 3.3	M5.5
706- 88		01 03 11.81	-11 26 50.37	17.9	12.621	12.048	11.667	9.68 ± 0.19	9.56 ± 0.19	9.25 ± 0.28	9.55 ± 0.22	41.3 ± 4.2	M5.5
194- 35		01 11 36.36	41 27 53.20	17.4	12.209	11.594	11.244	9.97 ± 0.19	9.72 ± 0.19	8.98 ± 0.28^b	9.84 ± 0.18	29.8 ± 2.5	M5.5
469-162 ^e		02 12 19.73	12 49 26.46	17.8	12.794	12.192	11.811	7.68 ± 0.35^a	7.30 ± 0.33	7.31 ± 0.32	7.42 ± 0.26	119.7 ± 14.3	M4.0
410- 38 ⁱ		02 30 24.88	16 48 26.29	16.7	11.843	11.258	10.949	18.0 ± 5.0	sdM6.0
245- 52		02 34 29.51	36 13 11.10	17.3	12.459	11.822	11.457	9.64 ± 0.19	9.42 ± 0.19	9.32 ± 0.28	9.49 ± 0.18	39.4 ± 3.2	M5.0
651- 2		02 43 13.83	-07 29 01.35	18.9	13.066	12.483	12.134	10.71 ± 0.19	10.62 ± 0.19	9.84 ± 0.28	10.51 ± 0.41	33.0 ± 6.1	M6.5
354-280 ^f		02 52 33.94	25 04 37.27	18.2	12.491	11.943	11.566	9.99 ± 0.19	9.30 ± 0.19	9.09 ± 0.28^a	9.54 ± 0.40	39.6 ± 7.3	M5.5
771- 50		02 56 27.00	-16 27 36.62	16.0	11.748	11.129	10.764	9.52 ± 0.19	9.38 ± 0.19	9.06 ± 0.28^a	9.38 ± 0.23	29.9 ± 3.1	M5.0
837- 37		03 06 01.73	-26 47 43.35	18.3	12.660	12.078	11.660	10.13 ± 0.19	10.02 ± 0.19	8.98 ± 0.28^b	10.07 ± 0.14	33.0 ± 2.2	M6.0
831- 39 ^g		03 12 27.53	-21 31 22.00	15.3	11.648	11.079	10.648	8.78 ± 0.19	8.73 ± 0.19	8.97 ± 0.28	8.79 ± 0.16	37.3 ± 2.7	M4.0
								7.78 ± 0.35	7.81 ± 0.33	8.02 ± 0.32	7.88 ± 0.22	57.0 ± 5.8	
247- 47		03 34 33.38	37 40 01.87	17.5	12.246	11.773	11.400	10.46 ± 0.19	10.25 ± 0.19	10.45 ± 0.28	10.37 ± 0.16	23.8 ± 1.7	M6.0
413- 28		03 40 54.92	19 29 47.44	18.8	13.194	12.605	12.232	10.02 ± 0.19	9.58 ± 0.19	7.70 ± 0.32^c	9.80 ± 0.26	48.1 ± 5.7	M5.5
301- 44		03 54 51.03	29 57 34.46	17.5	12.492	11.899	11.610	10.00 ± 0.19	9.00 ± 0.19^b	9.89 ± 0.28	9.97 ± 0.17	32.0 ± 2.5	M5.5
357-206		03 55 36.89	21 18 48.15	17.0	12.057	11.422	11.086	9.71 ± 0.19	9.51 ± 0.19	9.14 ± 0.28^a	9.52 ± 0.26	32.4 ± 3.9	M5.0
889- 13		03 55 47.79	-27 09 08.15	18.0	12.735	12.139	11.840	10.25 ± 0.19	9.85 ± 0.19	10.95 ± 0.28	10.22 ± 0.47	32.6 ± 7.0	M6.0
833- 40		04 06 52.38	-25 17 30.72	18.5	12.726	12.148	11.813	10.54 ± 0.19	10.26 ± 0.19	10.01 ± 0.28	10.33 ± 0.25	30.4 ± 3.5	M6.0
890- 9		04 16 31.15	-28 18 52.60	17.6	12.256	11.662	11.330	9.70 ± 0.19	9.37 ± 0.19	9.01 ± 0.28^a	9.44 ± 0.31	37.0 ± 5.2	M5.0
775- 35		04 38 47.47	-19 42 20.60	16.8	11.941	11.403	11.090	9.49 ± 0.19	9.25 ± 0.19	9.63 ± 0.28	9.42 ± 0.20	32.1 ± 2.9	M5.0
358-478 ^h		04 38 54.45	21 47 48.57	17.3	12.485	11.899	11.509	9.85 ± 0.19	9.54 ± 0.19	9.16 ± 0.28^a	9.59 ± 0.30	38.2 ± 5.3	M5.5
715- 41		04 39 04.93	-09 59 01.24	17.9	12.610	11.968	11.699	10.48 ± 0.19	9.85 ± 0.19	10.70 ± 0.28	10.26 ± 0.38	29.9 ± 5.2	M6.0
776- 7		04 44 46.17	-18 40 58.80	18.4	12.987	12.390	12.066	10.25 ± 0.19	9.99 ± 0.19	6.07 ± 0.32^c	10.12 ± 0.19	37.6 ± 3.2	M6.0
776- 26		04 52 27.95	-19 54 46.11	17.9	12.580	11.980	11.586	10.27 ± 0.19	9.99 ± 0.19	9.43 ± 0.28	10.00 ± 0.37	33.3 ± 5.6	M6.0
698- 18		21 37 17.33	-05 27 44.39	17.3	12.237	11.655	11.268	10.02 ± 0.19	9.50 ± 0.19	9.36 ± 0.28	9.68 ± 0.31	32.7 ± 4.6	M5.5
401- 24		22 58 04.47	27 30 36.48	17.8	12.762	12.096	11.811	10.12 ± 0.19	9.72 ± 0.19	9.09 ± 0.28^b	9.92 ± 0.24	37.2 ± 4.2	M5.5
702- 1 ⁱ		23 10 02.79	-06 05 53.37	18.4	13.004	12.405	12.017	10.15 ± 0.16	37.0 ± 5.0	M6.0:
702- 58		23 17 20.72	-02 36 32.41	17.2	12.304	11.662	11.275	9.89 ± 0.19	9.62 ± 0.19	9.27 ± 0.28	9.67 ± 0.28	34.0 ± 4.4	M5.5
878- 3	LHS 3970	23 33 40.57	-21 33 52.44	16.5	11.913	11.327	10.955	10.08 ± 0.19	9.79 ± 0.19	10.20 ± 0.28	9.98 ± 0.21	24.4 ± 2.4	M5.5
239- 33		23 38 55.41	43 00 15.27	16.8	11.945	11.367	11.042	9.59 ± 0.19	9.18 ± 0.19	9.03 ± 0.28^a	9.32 ± 0.26	33.8 ± 4.1	M5.0

Table 3—Continued

NLT/T/LP Name	Other Name	α (J2000)	δ	m_r	J	H	K_s	$M_J(\text{TiO 5})$	$M_J(\text{CaH 2})$	$M_J(\text{CaOH})$	M_J	d_{ph} (pc)	Sp. Type
880-140		23 59 03.90	-29 32 22.68	18.3	12.382	11.847	11.505	10.32 ± 0.19	9.93 ± 0.19	7.58 ± 0.32^c	10.13 ± 0.24	28.4 ± 3.1	M6.0

^aThis predicted value of M_J is double-valued and the result closest to the predictions based on other indices was used as our estimate M_J .

^bThis predicted value of M_J is double-valued and both predictions are more than 3σ from either of the other predictions. Neither are incorporated in calculating the final value M_J .

^cThis value is more than 3σ from either of the other predictions and was not used to estimate M_J .

^dLP 880-441 and LP 880-442 form a wide binary system with separation of $8''$. As with LP 31-301/302, the brighter star has indices which fall within the region of ambiguity in Figure 4. However, in this case the distance estimate to the fainter star is not sufficiently accurate to provide an improved distance estimate to the system.

^eHas common proper motion with G 4-5.

^fHas common proper motion with G 36-39.

^gHas common proper motion with LP 831-38.

^hHas common proper motion with G 8-48.

ⁱCandidate M subdwarf, see §§4.1 and 5.2

Note. — The columns are the same as the previous table.

Table 4. Regions That Define the Spectroscopic Indices

Index	Numerator (Å)	Denominator (Å)	Ref
CaOH	6230–6240	6345–6354	1
H α	6560–6566	6545–6555	1
CaH 1	6380–6390	Avg. of 6345–6355 and 6410–6430	1
CaH 2	6814–6846	7042–7046	1
CaH 3	6960–6990	7042–7046	1
TiO-a	7033–7048	7058–7073	2
TiO 2	7058–7061	7043–7046	1
TiO 3	7092–7097	7079–7084	1
TiO 4	7130–7135	7115–7120	1
TiO 5	7126–7135	7042–7046	1
VO-a	Sum of 7350–7370 and 7550–7570	7430–7470	2
PC3	8230–8270	7540–7580	3

References. — (1) Kirkpatrick et al. (1999); (2) PMSU1; (3) Martín et al. (1999)

Table 5. Spectral Indices for All Targets and Atandard

Name	2MASS Name	CaOH	H α	CaH 1	CaH 2	CaH 3	TiO-a	TiO 2	TiO 3	TiO 4	TiO 5	VO-a	PC3
LP 704- 48	2MASSI0006-0852	0.209	0.952	0.793	0.252	0.566	2.397	0.334	0.614	0.462	0.209	2.052	1.331
LP 880-442	2MASSI0007225-293526	0.411	0.933	0.807	0.429	0.686	1.484	0.616	0.705	0.663	0.421	1.917	0.912
LP 880-441	2MASSI0007225-293517	0.129	0.906	0.826	0.307	0.588	2.113	0.419	0.605	0.476	0.230	2.012	1.210
LP 824-383	2MASSI0012-2528	0.884	1.512	1.146	0.255	0.444	2.970	0.238	0.545	1.192	0.272	2.075	1.257
LP 292- 67	2MASSI0020+3305	0.316	0.942	0.787	0.333	0.654	2.123	0.416	0.555	0.542	0.251	2.070	1.207
LP 405- 5	2MASSI0021+1843	0.290	1.106	0.783	0.325	0.620	1.915	0.452	0.591	0.506	0.264	2.012	1.214
LP 645- 53	2MASSI0035-0541	0.330	0.989	0.858	0.368	0.685	1.873	0.468	0.621	0.542	0.292	2.025	1.106
LP 150- 53	2MASSI0053+4942	0.321	1.336	0.783	0.271	0.547	2.643	0.328	0.511	0.592	0.217	2.106	1.383
LP 150- 58	2MASSI0100+5055	0.295	1.585	0.795	0.305	0.603	2.261	0.372	0.562	0.530	0.245	2.032	1.172
LP 706- 88	2MASSI0103-1126	0.349	1.877	0.747	0.316	0.622	2.262	0.393	0.612	0.596	0.288	2.130	1.283
LP 647- 13	2MASSI0109-0343	0.559	2.050	0.969	0.497	0.791	1.691	0.555	0.794	0.826	0.504	2.369	1.947
LP 194- 35	2MASSI0111+4127	0.386	1.802	0.880	0.299	0.628	2.393	0.348	0.590	0.571	0.249	2.108	1.267
LP 467- 17	2MASSI0112+1502	0.332	0.906	0.883	0.347	0.687	2.040	0.427	0.599	0.531	0.261	2.054	1.177
LP 768-113	2MASSI0133-1738	0.417	1.198	0.790	0.438	0.686	1.459	0.621	0.714	0.641	0.438	1.960	0.882
LP 352- 79	2MASSI0203+2134	0.382	3.641	0.744	0.314	0.584	2.235	0.411	0.587	0.565	0.284	2.055	1.156
LP 469-162	2MASSI0212+1249	0.489	0.949	0.862	0.473	0.746	1.500	0.615	0.712	0.656	0.428	1.952	0.966
LP 649- 72	2MASSI0214-0357	0.312	1.862	0.799	0.315	0.621	2.297	0.370	0.569	0.545	0.250	2.065	1.181
LP 649- 93	2MASSI0218-0617	0.437	1.512	1.035	0.300	0.603	2.842	0.319	0.386	0.497	0.220	2.202	1.411
LP 410- 38	2MASSI0230+1648	0.286	1.962	0.627	0.243	0.480	2.250	0.396	0.523	0.580	0.246	2.019	1.290
LP 245- 52	2MASSI0234+3613	0.339	1.769	0.785	0.331	0.602	2.158	0.417	0.623	0.585	0.294	2.066	1.289
G 75-35	2MASSI0241-0432	0.372	1.329	0.763	0.395	0.647	1.674	0.551	0.652	0.596	0.381	1.981	0.932
LP 651- 2	2MASSI0243-0729	0.268	1.192	0.863	0.202	0.532	2.764	0.301	0.497	0.391	0.150	2.137	1.176
LP 651- 17	2MASSI0250-0808	0.293	1.380	0.868	0.318	0.640	2.199	0.405	0.583	0.550	0.251	2.111	1.218
LP 354-280	2MASSI0252+2504	0.371	0.995	0.883	0.344	0.681	2.265	0.442	0.563	0.510	0.247	2.032	1.022

Table 5—Continued

Name	2MASS Name	CaOH	H α	CaH 1	CaH 2	CaH 3	TiO-a	TiO 2	TiO 3	TiO 4	TiO 5	VO-a	PC3
LP 771- 50	2MASSI0256-1627	0.375	1.565	0.768	0.335	0.599	2.094	0.442	0.630	0.593	0.310	2.025	1.141
LP 299- 15	2MASSI0305+2742	0.362	1.862	0.774	0.331	0.608	2.172	0.427	0.609	0.581	0.306	2.027	1.255
LP 837- 37	2MASSI0306-2647	0.386	4.255	0.754	0.266	0.541	3.264	0.263	0.543	0.665	0.228	2.132	1.354
LP 831- 39	2MASSI0312-2131	0.387	1.050	0.782	0.405	0.654	1.488	0.597	0.779	0.619	0.410	1.944	0.891
LP 888- 18	2MASSI0331-3042	0.570	2.029	1.017	0.284	0.567	3.113	0.286	0.598	0.559	0.217	2.208	1.707
LP 247- 47	2MASSI0334+3740	0.184	0.920	0.733	0.242	0.580	2.566	0.324	0.613	0.454	0.183	2.096	1.340
LP 247- 56	2MASSI0338+3828	0.324	1.023	0.770	0.328	0.635	1.937	0.444	0.620	0.520	0.273	2.025	1.184
LP 413- 28	2MASSI0340+1929	0.432	1.464	0.803	0.314	0.624	2.354	0.359	0.416	0.553	0.243	2.071	1.413
LP 413- 53	2MASSI0350+1818	0.692	2.254	0.942	0.319	0.754	2.605	0.358	0.576	0.694	0.292	2.180	1.554
LP 301- 44	2MASSI0354+2957	0.261	1.149	0.756	0.376	0.551	2.208	0.381	0.536	0.527	0.245	2.047	1.247
LP 357-206	2MASSI0355+2118	0.364	1.699	0.813	0.321	0.617	2.205	0.405	0.636	0.571	0.284	2.047	1.236
LP 889- 13	2MASSI0355-2709	0.117	1.207	1.262	0.285	0.655	2.342	0.405	0.464	0.397	0.212	2.152	1.129
LP 31-301	2MASSI0405574+711641	0.423	1.001	0.808	0.424	0.687	1.523	0.588	0.696	0.621	0.396	1.974	1.019
LP 31-302	2MASSI0405565+711639	0.291	1.854	0.803	0.314	0.597	2.159	0.414	0.601	0.577	0.291	2.026	1.225
LP 833- 40	2MASSI0406-2517	0.245	1.085	0.717	0.241	0.452	2.291	0.380	0.345	0.459	0.172	2.072	1.388
LP 714- 37	2MASSI0410-1251	0.320	1.306	0.815	0.328	0.635	2.119	0.403	0.597	0.512	0.259	2.059	1.230
LP 890- 2	2MASSI0413-2704	0.297	2.672	0.841	0.277	0.593	2.572	0.297	0.563	0.533	0.228	2.106	1.372
LP 890- 9	2MASSI0416-2818	0.383	0.990	0.857	0.336	0.649	2.062	0.468	0.565	0.572	0.286	2.008	1.224
LP 775- 31	2MASSI0435-1606	0.277	1.444	0.870	0.249	0.545	3.027	0.316	0.558	0.541	0.210	2.201	1.598
LP 775- 35	2MASSI0438-1942	0.297	0.963	0.853	0.349	0.664	1.901	0.510	0.604	0.489	0.314	2.019	0.962
LP 358-478	2MASSI0438+2147	0.361	1.647	0.802	0.318	0.598	2.068	0.428	0.670	0.571	0.266	2.032	1.247
LP 715- 41	2MASSI0439-0959	0.151	1.925	0.811	0.285	0.497	2.712	0.349	0.571	0.422	0.181	2.029	1.197
LP 415-302	2MASSI0439+1615	0.292	1.171	0.803	0.321	0.611	1.993	0.429	0.589	0.522	0.264	2.013	1.040
LP 655- 48	2MASSI0440-0530	0.357	2.460	0.877	0.284	0.597	2.918	0.303	0.613	0.597	0.245	2.205	1.658

Table 5—Continued

Name	2MASS Name	CaOH	H α	CaH 1	CaH 2	CaH 3	TiO-a	TiO 2	TiO 3	TiO 4	TiO 5	VO-a	PC3
LP 776- 7	2MASSI0444-1840	0.736	1.032	0.840	0.270	0.601	2.114	0.365	0.448	0.577	0.212	2.144	1.221
LP 716- 10	2MASSI0452-1058	0.256	0.943	0.841	0.333	0.648	1.974	0.436	0.571	0.500	0.252	2.051	1.195
LP 776- 26	2MASSI0452-1954	0.324	1.327	0.762	0.269	0.579	2.593	0.347	0.464	0.534	0.209	2.049	1.229
LP 396- 18	2MASSI2102+2237	0.416	0.939	0.828	0.426	0.708	1.613	0.548	0.678	0.610	0.369	1.984	1.068
LP 397- 10	2MASSI2116+2238	0.305	1.434	0.805	0.288	0.607	2.456	0.354	0.526	0.524	0.232	2.090	1.334
LP 817- 54	2MASSI2129-1855	0.312	0.983	0.872	0.334	0.653	1.970	0.457	0.561	0.575	0.294	2.047	1.164
LP 698- 2	2MASSI2132-0511	0.338	1.059	0.868	0.331	0.688	2.047	0.458	0.555	0.552	0.264	2.098	1.109
LP 698- 18	2MASSI2137-0527	0.334	0.940	0.875	0.322	0.620	2.092	0.417	0.541	0.506	0.243	2.062	1.184
LP 638- 50	2MASSI2151-0127	0.299	1.332	0.787	0.307	0.588	2.133	0.400	0.583	0.514	0.270	2.033	1.091
LP 288- 40	2MASSI2236+3655	0.325	0.968	0.771	0.365	0.631	1.701	0.511	0.623	0.588	0.320	1.968	1.116
LP 521- 18	2MASSI2248+1232	0.326	1.709	0.777	0.318	0.593	2.347	0.387	0.613	0.561	0.271	2.047	1.220
LP 401- 10	2MASSI2254+2527	0.352	2.022	0.804	0.289	0.573	2.430	0.352	0.556	0.561	0.259	2.074	1.263
LP 401- 24	2MASSI2258+2730	0.371	0.771	0.794	0.299	0.624	2.197	0.393	0.554	0.440	0.229	2.056	1.237
LP 701- 59	2MASSI2301-0539	0.501	0.975	0.804	0.461	0.756	1.516	0.622	0.697	0.628	0.422	1.954	0.969
LP 702- 1	2MASSI2310-0605	0.287	0.867	0.696	0.287	0.611	2.445	0.414	0.550	1.155	0.399	2.123	1.255
LP 702- 58	2MASSI2317-0236	0.347	1.704	0.811	0.309	0.610	2.444	0.363	0.599	0.579	0.260	2.042	1.173
LP 934- 33	2MASSI2322-2725	0.374	1.668	0.793	0.299	0.561	2.306	0.385	0.600	0.520	0.259	2.015	1.239
LP 878- 90	2MASSI2323-2232	0.478	0.995	0.810	0.495	0.733	1.341	0.674	0.752	0.702	0.517	1.946	0.944
LP 878- 3	2MASSI2333-2133	0.219	0.958	0.779	0.291	0.602	2.196	0.407	0.528	0.499	0.234	2.056	1.148
LP 763- 38	2MASSI2337-0838	0.432	2.084	1.089	0.271	0.574	2.916	0.265	0.460	0.373	0.175	2.277	1.489
LP 763- 3	2MASSI2337-1250	0.312	1.870	0.779	0.296	0.576	2.502	0.355	0.557	0.543	0.245	2.052	1.190
LP 239- 33	2MASSI2338+4300	0.379	0.926	0.744	0.357	0.631	1.733	0.491	0.595	0.541	0.301	1.991	1.133
LP 239- 52	2MASSI2347+4238	0.332	0.926	0.837	0.360	0.671	1.857	0.492	0.609	0.558	0.296	2.026	1.168
LP 880-140	2MASSI2359-2932	0.449	0.914	0.896	0.276	0.594	2.811	0.307	0.460	0.413	0.202	2.071	1.301

Table 5—Continued

Name	2MASS	CaOH	H α	CaH 1	CaH 2	CaH 3	TiO-a	TiO 2	TiO 3	TiO 4	TiO 5	VO-a	PC3
	Name												
DG ERI		0.480	0.955	0.998	0.547	0.864	1.796	0.543	0.649	0.683	0.396	1.910	0.959
GJ 1224		0.347	1.586	0.755	0.359	0.621	1.807	0.498	0.621	0.586	0.338	1.988	1.162
GJ 1227		0.373	0.950	0.803	0.391	0.668	1.672	0.534	0.648	0.589	0.343	1.973	1.091
GJ 1245		0.298	1.287	0.753	0.308	0.575	2.136	0.415	0.573	0.556	0.274	2.050	1.287
GL 643		0.399	0.980	0.780	0.430	0.685	1.456	0.643	0.694	0.639	0.432	1.966	1.071
GL 699		0.387	0.949	0.761	0.400	0.654	1.472	0.608	0.715	0.608	0.400	1.963	0.990
GL 720B		0.416	0.957	0.827	0.440	0.697	1.485	0.611	0.724	0.621	0.401	1.947	0.881
GL 752A		0.531	0.969	0.836	0.545	0.780	1.308	0.730	0.764	0.730	0.554	1.949	0.894
GL 83.1		0.332	1.136	0.773	0.362	0.619	1.691	0.537	0.649	0.592	0.345	2.003	1.003
LHS 3406		0.288	2.656	0.599	0.307	0.676	2.484	0.400	0.305	0.590	0.266	2.253	1.260
LHS 1326		0.239	1.017	0.779	0.299	0.618	2.200	0.423	0.572	0.517	0.262	2.044	1.229
LHS 17		0.257	0.935	0.794	0.285	0.581	1.966	0.430	0.511	0.467	0.243	1.979	1.151
VB 10		0.515	1.310	0.948	0.343	0.643	2.410	0.383	0.656	0.661	0.304	2.297	1.767
VB 8		0.277	1.386	0.759	0.225	0.497	3.214	0.291	0.495	0.489	0.167	2.143	1.627

Table 6. Activity

Name	2MASS Name	H α flux $10^{-15} \text{ergs } cm^{-2} sec^{-1}$	H α EW (Å)	m_{bol}	$\log \frac{F_\alpha}{F_{bol}}$
LP 405- 5	2MASSI0021+1843	5.51	2.3	13.27	-4.36
LP 150- 53	2MASSI0053+4942	0.85	4.2	14.95	-4.50
LP 150- 58	2MASSI0100+5055	4.58	6.4	14.41	-3.99
LP 706- 88	2MASSI0103-1126	2.67	8.2	14.53	-4.17
LP 647- 13	2MASSI0109-0343	2.75	10.5	13.60	-4.53
LP 194- 35	2MASSI0111+4127	4.98	9.0	14.14	-4.06
LP 768-113	2MASSI0133-1738	249.00	2.0	10.70	-3.74
LP 352- 79	2MASSI0203+2134	61.80	26.0	13.54	-3.21
LP 649- 72	2MASSI0214-0357	31.00	9.2	12.40	-3.96
LP 649-93	2MASSI0218-0617	1.03	3.0	14.87	-4.45
LP 410- 38	2MASSI0230+1648	12.63	10.2	13.77	-3.80
LP 245- 52	2MASSI0234+3613	2.93	7.9	14.36	-4.20
G 75-35	2MASSI0241-0432	257.00	3.7	11.03	-3.59
LP 651- 2	2MASSI0243-0729	0.92	1.5	15.04	-4.43
LP 651- 17	2MASSI0250-0808	3.02	3.7	13.81	-4.41
LP 354-280	2MASSI0252+2504	0.27	0.6	14.42	-5.21
LP 771- 50	2MASSI0256-1627	6.84	5.9	13.64	-4.12
LP 299- 15	2MASSI0305+2742	9.05	8.1	13.50	-4.06
LP 837- 37	2MASSI0306-2647	6.39	30.3	14.60	-3.77
LP 831-39	2MASSI0312-2131	2.15	0.90	13.50	-4.68
LP 888- 18	2MASSI0331-3042	2.22	8.9	13.31	-4.74
LP 413- 28	2MASSI0340+1929	0.59	5.5	15.12	-4.59
LP 413- 53	2MASSI0350+1818	0.76	5.7	14.85	-4.59
LP 301-44	2MASSI0354+2957	1.18	2.3	14.42	-4.57
LP 357-206	2MASSI0355+2118	5.01	7.6	13.97	-4.13
LP 31-302	2MASSI0405565+711638	33.30	8.9	12.03	-4.08
LP 714- 37	2MASSI0410-1251	9.06	4.3	12.98	-4.26
LP 890- 2	2MASSI0413-2704	5.39	16.0	14.16	-4.02
LP 775- 31	2MASSI0435-1606	8.51	7.0	12.35	-4.54
LP 358-478	2MASSI0438+2147	3.48	6.0	14.39	-4.12
LP 715- 41	2MASSI0439-0959	11.20	9.1	14.57	-3.54
LP 415-302	2MASSI0439+1615	63.50	2.9	12.04	-3.79
LP 655- 48	2MASSI0440-0530	10.80	13.2	12.61	-4.34
LP 776- 7	2MASSI0444-1840	0.66	0.9	14.94	-4.62
LP 776- 26	2MASSI0452-1954	1.09	3.2	14.51	-4.57
LP 397- 10	2MASSI2116+2238	3.74	4.4	13.73	-4.35
LP 638- 50	2MASSI2151-0127	12.20	3.1	13.23	-4.03

Table 6—Continued

Name	2MASS Name	H α flux $10^{-15} \text{ergs } cm^{-2} sec^{-1}$	H α EW (Å)	m_{bol}	$\log \frac{F_\alpha}{F_{bol}}$
LP 521- 18	2MASSI2248+1232	11.90	6.9	13.13	-4.09
LP 401-10	2MASSI2254+2527	8.18	9.9	13.56	-4.08
LP 702- 58	2MASSI2317-0236	4.26	7.4	13.11	-4.54
LP 934-33	2MASSI2322-2725	4.99	6.6	13.52	-4.31
LP 763- 38	2MASSI2337-0838	2.37	9.0	14.22	-4.35
LP 763- 3	2MASSI2337-1250	2.74	11.6	13.39	-4.62

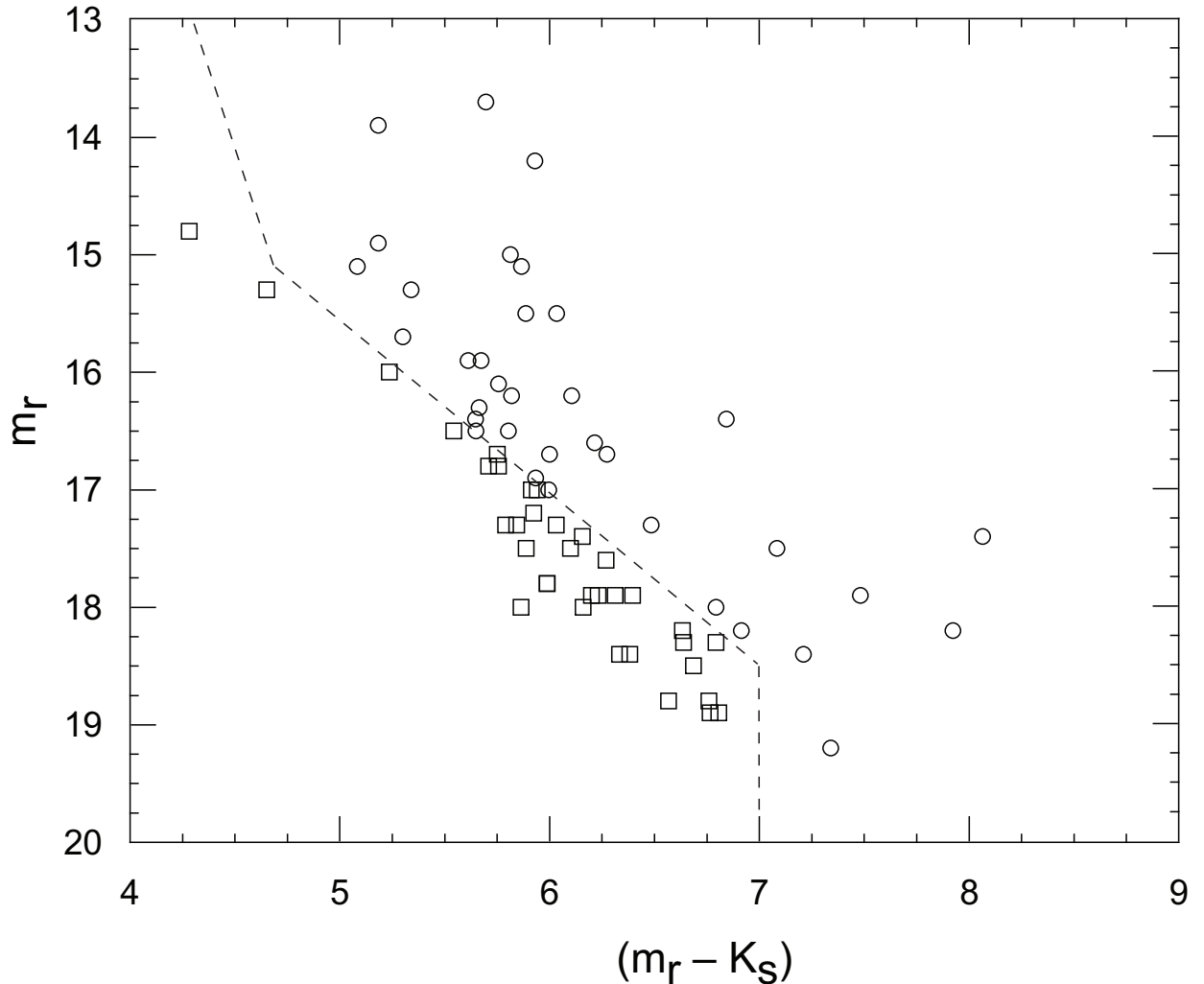


Fig. 1.— Our 70 objects in the $(m_r, m_r - K_s)$ plane. Circles are objects that are included in NLTT Sample 1 described in Paper I. Squares are not in the finalized sample. The dashed line marks the limits, $m_r(\text{lim})$, for NLTT Sample 1.

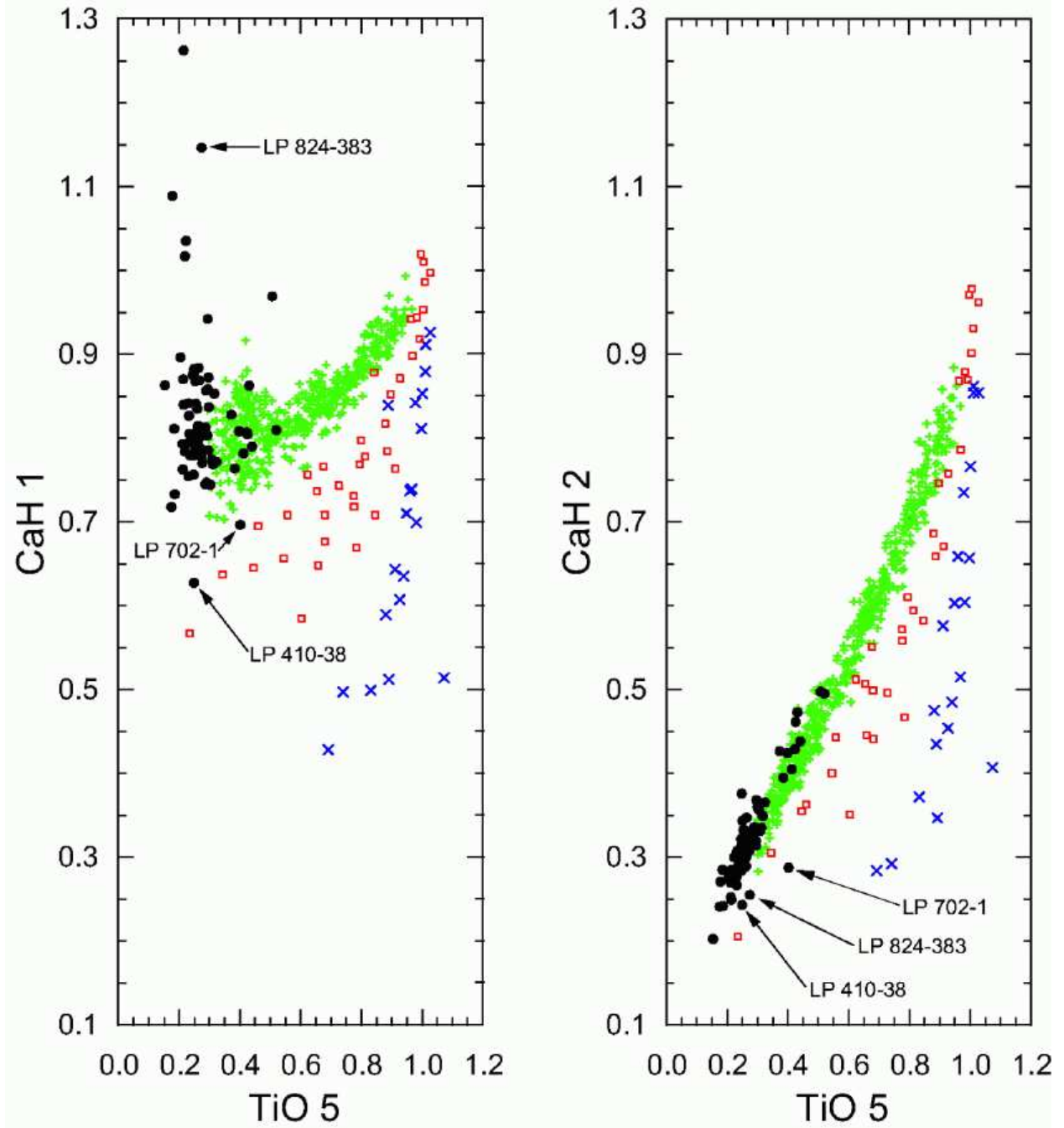


Fig. 2.— Comparison between the CaH and TiO 5 band-strengths measured from our observations of NLTT dwarfs and standard stars. The green plus signs mark data for disk dwarfs from PMSU1; open red squares are sdM subdwarfs and blue crosses are esdM subdwarfs from Gizis (1997); our observations are plotted as solid black circles. Three possible M subdwarfs are identified. As discussed in the text (§§4.1 and 5.2), both LP 824-383 and LP 702-1 have low signal-to-noise spectra and are probably not metal poor.

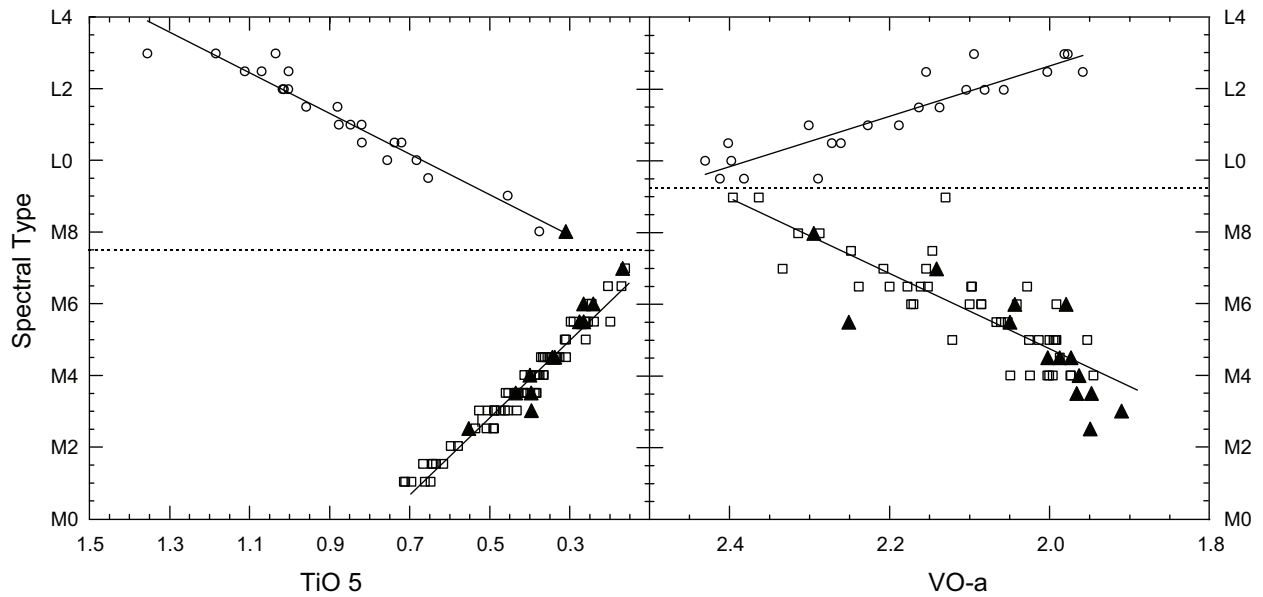


Fig. 3.— TiO 5 and VO-a spectral type calibrations. Late-type calibrating objects (later than M7 for TiO 5 and M9 for VO-a) are plotted as open circles, earlier types as open squares, and our standards as solid triangles. The dotted line illustrates the separation of the two trends. Data are from PMSU1 and Kirkpatrick et al. (2000). In addition, our standards were included in calculating the late-type TiO 5 and early-type VO-a relations. The early TiO 5 relation was adopted from PMSU1 and our standards are overplotted to show their agreement.

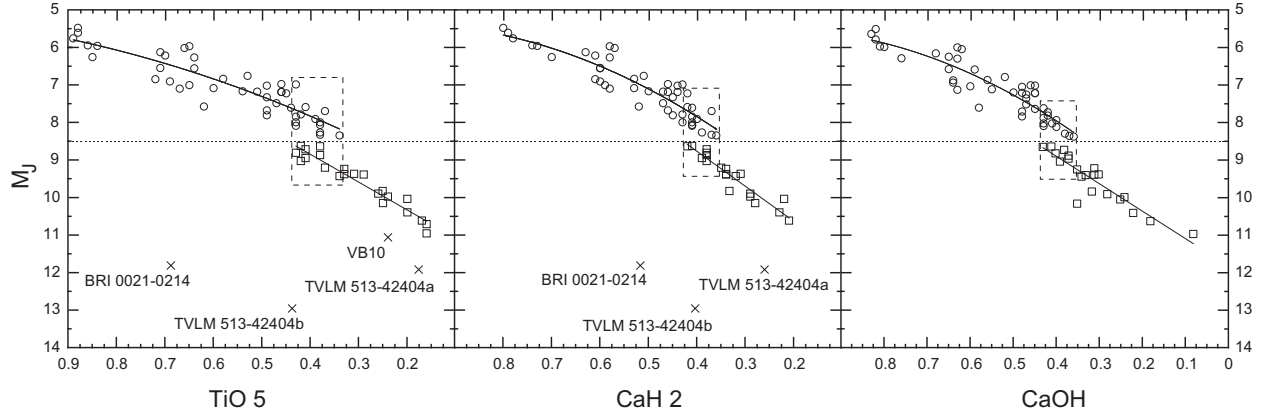


Fig. 4.— Absolute magnitude calibration using K7 and later dwarfs. Circles are the data included in the calibration for brighter objects while the fainter calibration objects are plotted as squares. The dashed boxed regions ($0.34 \leq TiO\ 5 \leq 0.43$, $0.36 \leq CaH\ 2 \leq 0.42$, $0.36 \leq CaOH \leq 0.43$) show where the calibration is double-valued. The crosses, VB 10 (M8), TVLM 513-42404a (M7), TVLM 513-42404b (M9), and BRI 0021-0214 (M9.5), show that the trends reverse for later types.

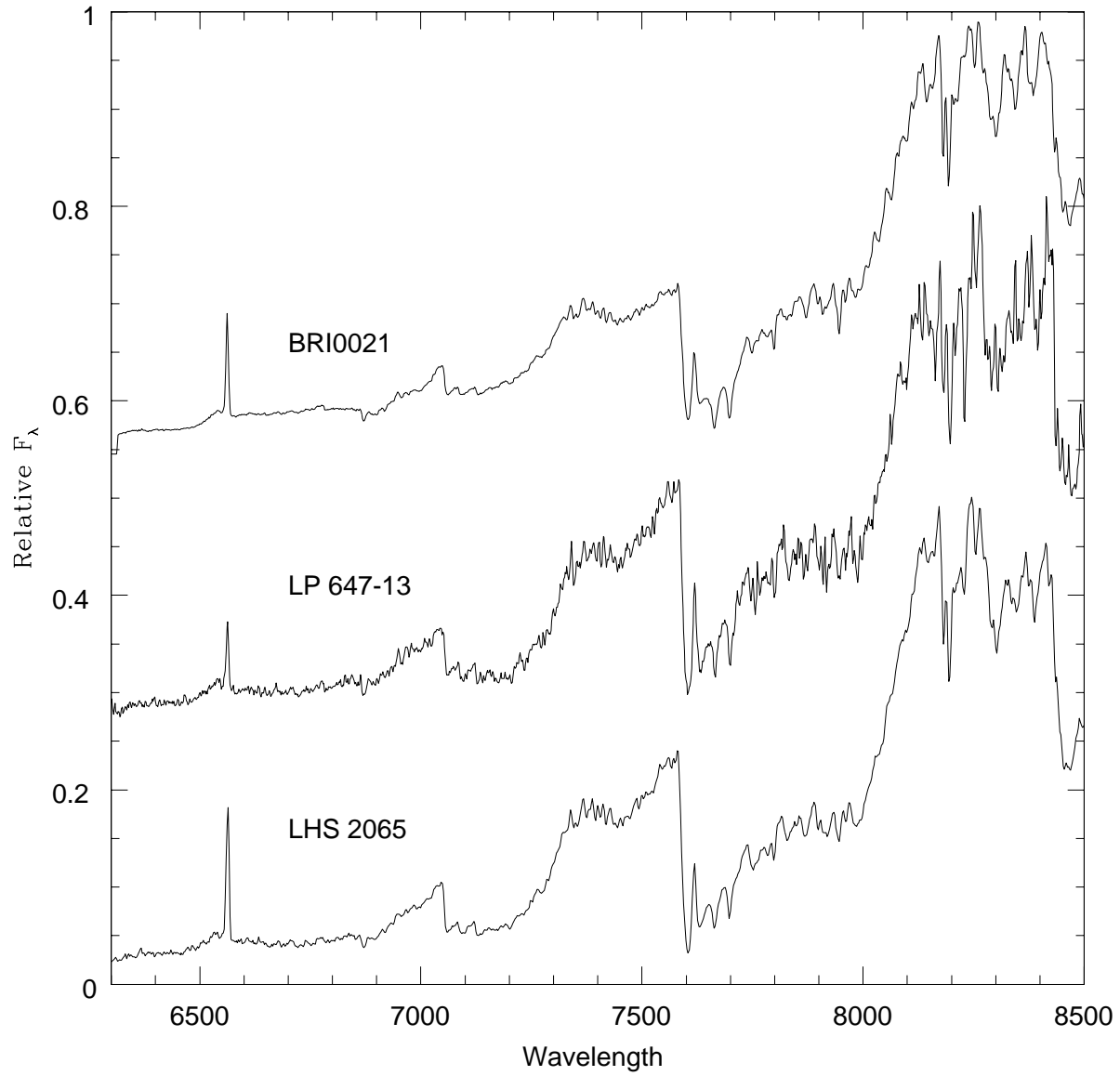


Fig. 5.— Spectrum of LP 647-13, an M9 dwarf at 10.5 pc. Keck LRIS spectra of the M9 and M9.5 standards, LHS 2065 and BRI 0021-0214, are shown for comparison.

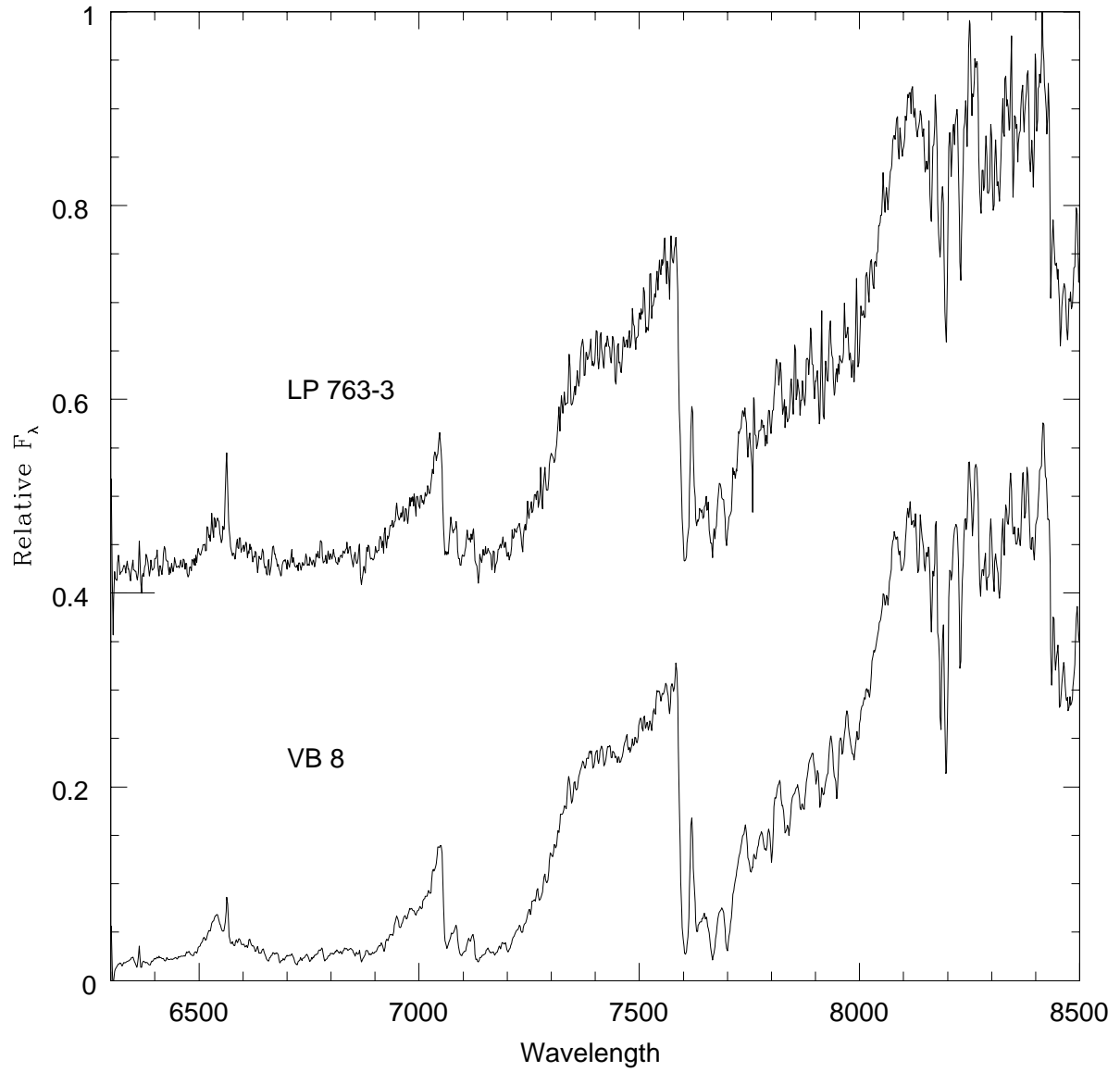


Fig. 6.— Spectrum of the M7 dwarf, LP 763-3. The spectrum of the M7 standard, VB 8, is shown for comparison.

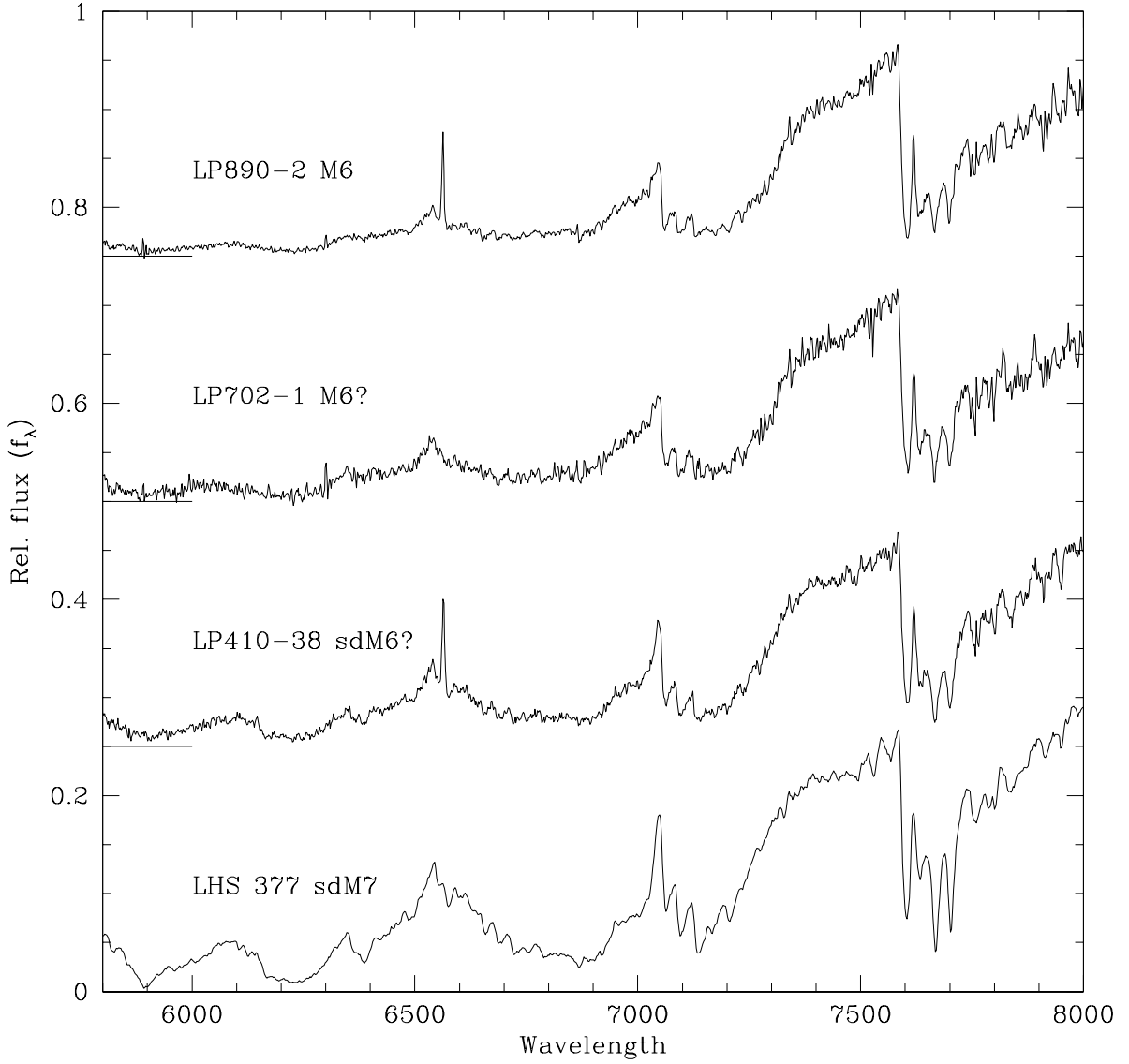


Fig. 7.— A comparison between our spectra of the two subdwarf candidates, LP 702-1 and LP 410-38, and data for an M6 dwarf (LP 890-2) and the late-type intermediate subdwarf, LHS 377 (a Keck LRIS spectrum). As discussed in the text, while LP 702-1 is probably misclassified due to the relatively low signal-to-noise ratio, LP 410-38 shows the enhanced hydride absorption characteristic of mildly metal-poor subdwarfs.

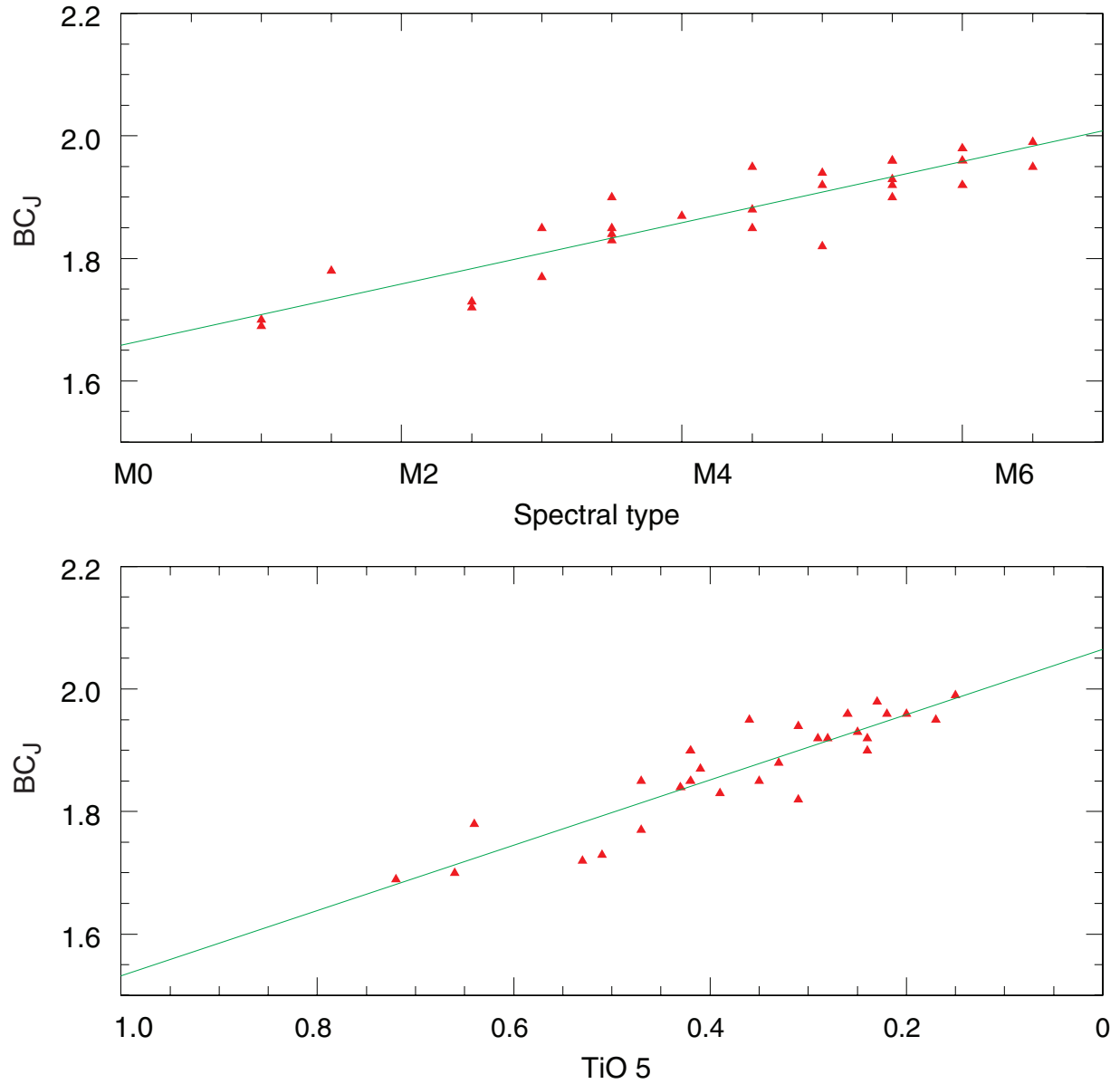


Fig. 8.— J -band bolometric correction as a function of spectral type and TiO 5 index for M0 to M7 dwarfs based on data from Leggett et al. (2000).

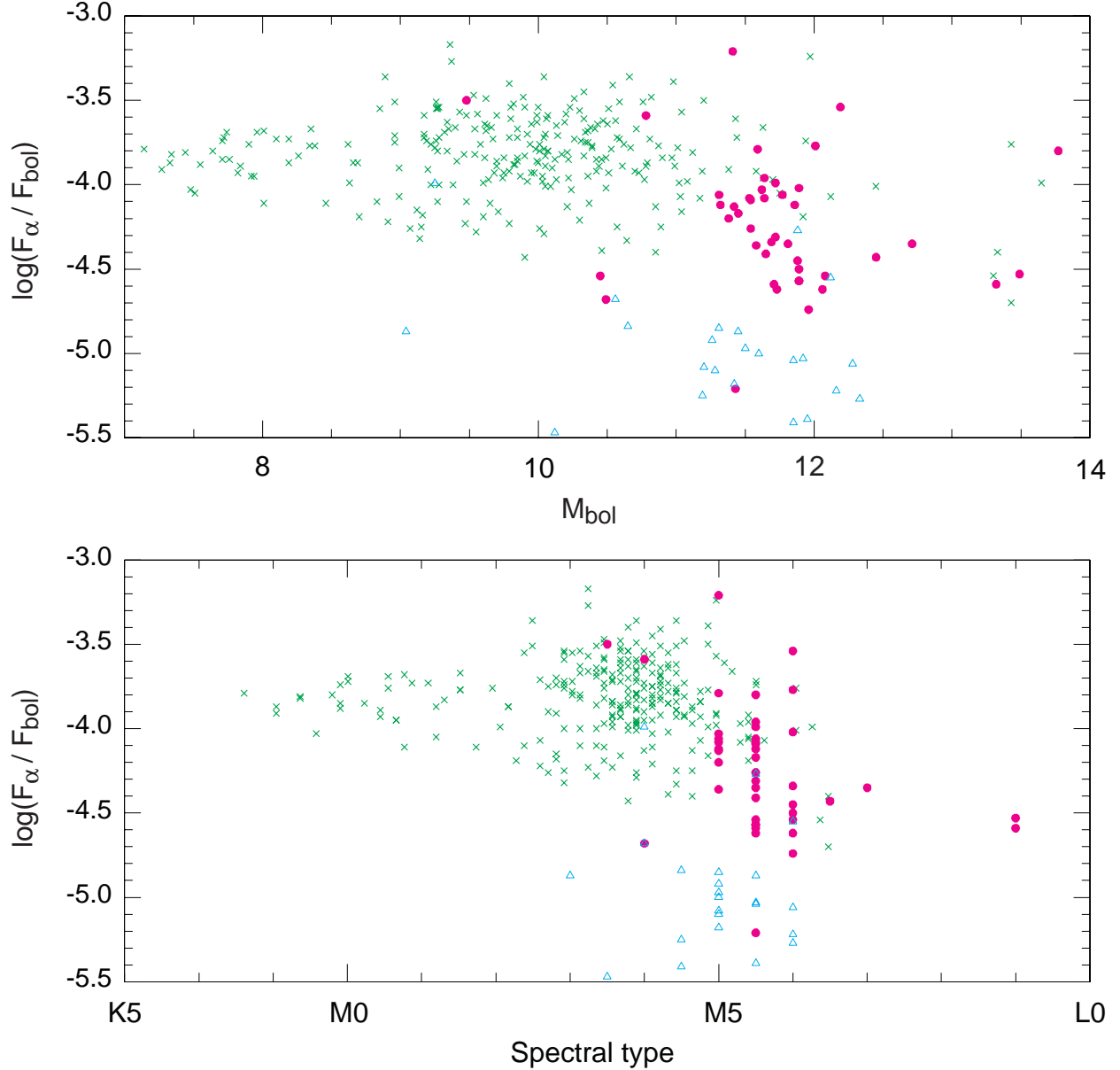


Fig. 9.— Distribution of chromospheric activity amongst the NLTT M dwarf sample, plotted against M_{bol} (top) and spectral type (bottom). Data for nearby dMe stars from the PMSU2 sample are plotted as green crosses; NLTT dwarfs with detected $H\alpha$ emission in the present sample are plotted as solid magenta circles; open blue triangles mark upper limits for the remaining NLTT dwarfs.